Supporting Information

Selective Monoborylation of Methane by Metal-Organic Framework Confined Mononuclear Pyridylimine-Iridium(I) Hydride

Rahul Kalita,[a] Manav Chauhan,[a] Poorvi Gupta,[a] Wahida Begum,[a] Chhaya Thadhani,[a] Biplab Ghosh,[b] Balendra,[a] Himani Bisht,[a] Kuntal Manna*[a]

[a]Department of Chemistry, Indian Institute of Technology Delhi, Hauz Khas, New Delhi 110016, India
[b]BARC Beamlines Section, Indus-2, RRCAT, Indore 452013, India

*Email: kmanna@chemistry.iitd.ac.in

Table of contents

1. General experiment. All the experiments were performed under inert conditions inside the glovebox, except if any case was demonstrated. All the solvents were purchased from Finar and used without further purification. Tetrahydrofuran and cyclohexane were dried with calcium hydride followed by distillation over Na/benzophenone. All the reagents are commercially available and used directly as received. 2,5-Dibromoaniline was purchased from Alfa Aesar, $IrCl_3.3H_2O$ was purchased from TCI chemicals and $ZrCl_4$ was purchased from GLR Innovations. ^1H NMR spectra were recorded on a Bruker NMR 500 DRX spectrometer at 500 MHz and referenced to the proton resonance resulting from DMSO-d_6 (δ 2.5) and $CDCl_3$ (δ 7.26). Thermogravimetric analysis (TGA) was performed on a PerkinElmer TGA7 system on well-ground samples under the flowing nitrogen atmosphere with a heating rate of 10 °C/min with a range of 40-800 °C. Room temperature powder X-ray diffraction data were collected on a Bruker Advance diffractometer using Ni-filtered Cu Kα radiation (λ = 1.5406 Å). Data were collected with a step size of 0.05° and at count time of 1s per step over the range 4°<2θ<70°. The experimental and simulated PXRD patterns are in good agreement indicating the monophasic nature of the bulk samples. For powder X-ray diffraction measurement of MOFs, moist sample was mounted on a PXRD groove. After catalysis, pyrim-UiO-Ir was recovered after centrifugation and stored in THF. Just before the PXRD measurement, the THF was removed, and the moist sample was mounted on a PXRD groove. The catalysis was carried out without any mechanical stirring, and the recovered MOF was not dried before the measurement of PXRD to prevent any mechanical degradation and pore collapse of the MOF. The liquid phase of catalytic reactions was determined by gas chromatograph using Agilent 7890B gas chromatograph equipped with flame ionisation detector (FID) and mass detector (Agilent 5977B GC/MSD). The following chromatographic conditions were employed; carrier gas: He, N_2, flow rate: 1 mL min^{-1}, injection volume: 5.0 µL, column oven temperature was initially 40.0 °C and then increased up to 240 ℃ with the rate of 5 ºC per minute, and detector temperature was 250 ℃. ICP-OES data were obtained with an Agilent 5110 ICP-OES and analyzed using Dichroic Spectral Combiner (DSC). Samples were diluted in a 5% HNO_3 matrix and analyzed with a four-point standard curve over the range from 1 ppm to 10 ppm. The correlation coefficient was >0.9990 for all analytes of interest. All the borylation reactions were performed using 100 mL Parr pressure vessels [4793 (VGR)-T-SS-3000-DVD]. The vessel was pressurized directly from a CH_4 gas tank using a gauge (0-3000 psi displayed, 0-200 bar). To analyse the chemical state of transition elements, XPS were recorded on an X-ray photoelectron spectrometer, PHI 5000 VersaProbe III using Al-Kα ($h\nu$ = 1486.6 eV) X-ray source. MOF samples were vacuum dried at room temperature, and then powder samples were measured ultra-high vacuum environment. Surface area and pore volume were measured with a BELLSORP MAX II-high performance gas and vapor adsorption system with three microporous ports. For BET surface area measurement, MOF sample was first dried via freeze-drying method. For freeze-drying, MOF was first soaked with benzene. Then, the MOF slurry was frozen at -10 °C and dried slowly under vacuum at the same temperature. Then, samples were degassed under vacuum at 80 °C for 24 h before measurement. The morphology and chemical compositions were analysed with a Ziess Fe-SEM ultra plus55 operating at 20 KV. After vacuum drying, a very small amount of the powder samples of MOF (1-2 mg) were dispersed on the carbon tape for FE-SEM imaging. Infra-red (IR) spectra of samples were recorded with FT-IR Spectrometer (MS-632). The MOF samples were vacuum dried at 100 °C to remove the moisture, which was then taken inside the glovebox, and a KBr pellet of powder sample was made. The pellets were kept in inert conditions and IR was recorded under a nitrogen atmosphere.

2. Synthesis and characterization of pyridylimine-functionalized UiO-68 MOFs.

2.1. Synthesis of UiO-68-NH_2 MOF.[1]

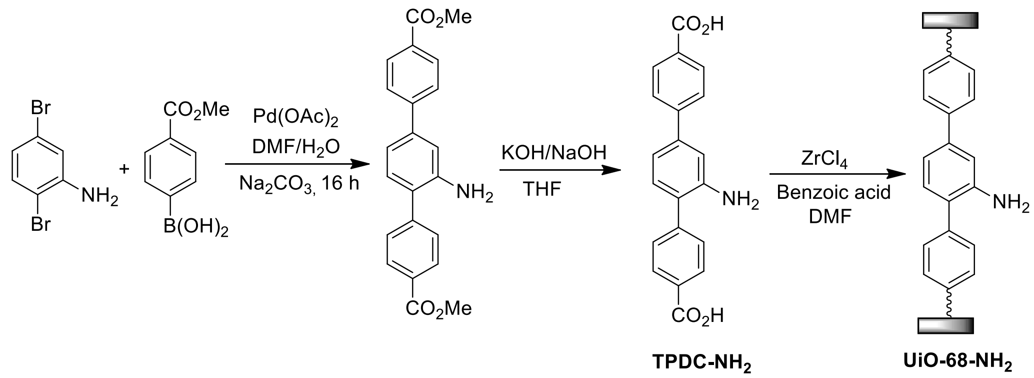

In a 10 mL glass vial, TPDC-NH_2 (2'-amino-[1,1':4',1''-terphenyl]-4,4''-dicarboxylic acid) ligand (0.010 g, 0.03 mmol), which was synthesized with the help modified procedure[2,3], and benzoic acid (0.073 g, 0.6 mmol) were dissolved in a DMF solution (1.22 mL) followed by the addition of $ZrCl_4$ (0.007 g, 0.03 mmol). The resulting mixture was sonicated for few minutes and then kept it in a preheated oven at 70 °C for 3 d. After cooling to room temperature, the crystalline solid was isolated by centrifugation and washed it by DMF several times to afford UiO-68-NH_2 MOFs in 41% yield.

2.2. Synthesis of pyrim-UiO MOFs via post-synthetic modification of UiO-68-NH_2 MOFs.[4]

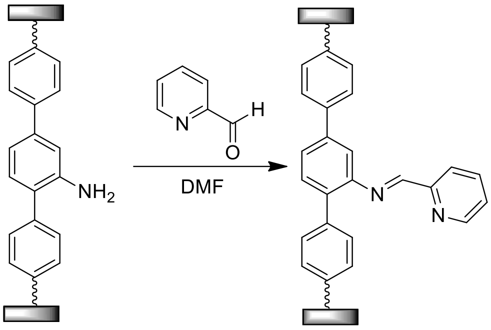

In a centrifuge tube inside the glovebox, UiO-68-NH_2 MOF (0.017 g, 0.006 mmol) was added in 1 mL DMF followed by the addition of 2-pyridinecarboxaldehyde (4 µL, 0.04 mmol). It was then left overnight with periodic shaking. The resultant solid was washed multiple times with DMF to obtain pyrim-UiO-68 MOF as a light brown solid.

2.2.1. Analysis of digested pyrim-UiO MOFs by ^{1}H NMR. Sample of pyrim-UiO MOF was charged in a vial containing 0.5 mL of DMSO-d_6, and then 0.5 mL saturated solution of K_3PO_4 in D_2O was added to it and mixed well. The top organic layer was taken and analyzed by ^{1}H NMR.

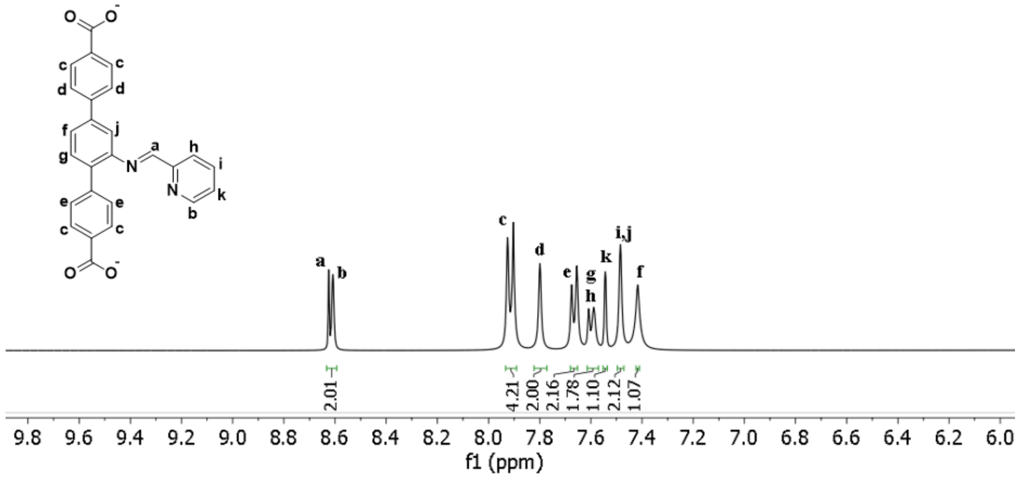

Figure S1. ^{1}H NMR spectrum (500 MHz, DMSO-d_6) of pyrim-UiO MOF digested in K_3PO_4/D_2O/DMSO-d_6.

3. Post synthetic metalation of pyrim-MOF.[5]

3.1. Synthesis of pyrim-UiO-$IrCl_3$.

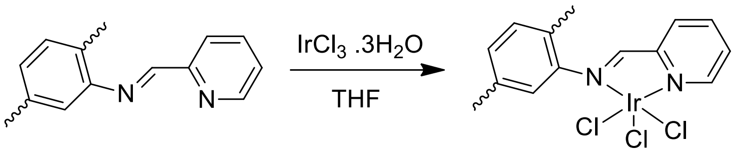

Pyrim-UiO MOF (0.030 g, 0.009 mmol) in THF was charged into a vial to which a 1 mL THF solution of $IrCl_3.3H_2O$ (0.019 g, 0.054 mmol was added. The mixture was stirred slowly overnight at room temperature. The resultant solid was centrifuged out of suspension and washed with THF 4-5 times. Pyrim-UiO-$IrCl_3$ has 28% solvent weight based on TGA analysis and 32% Ir-loading based on ICP-OES analysis.

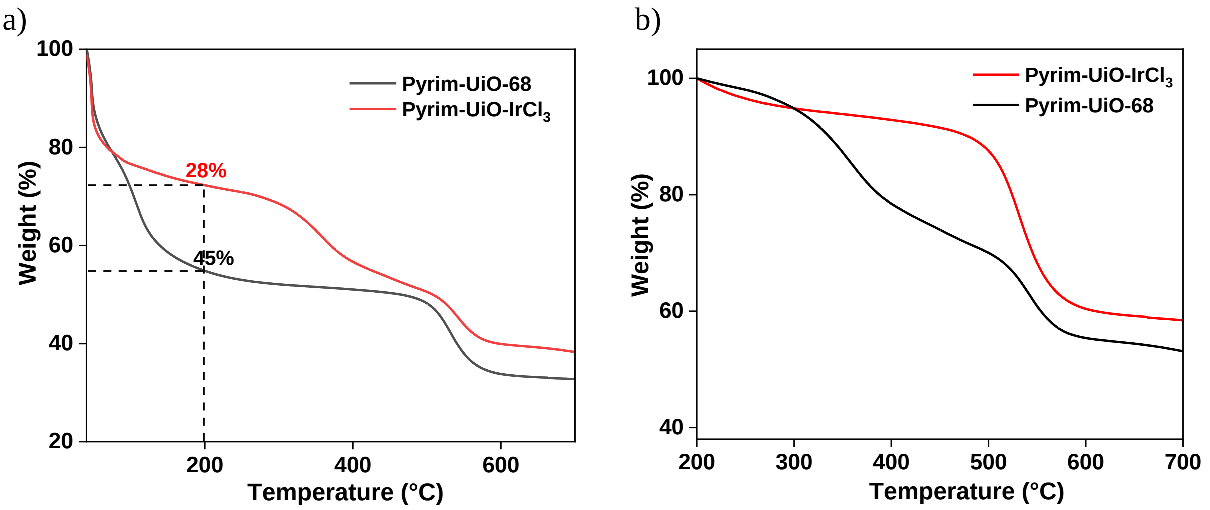

Figure S2. (a) TGA curve of freshly prepared pyrim-UiO-68 and pyrim-UiO-$IrCl_3$. A solvent weight loss of 45% was observed in pyrim-UiO-68 and 28% in pyrim-UiO-$IrCl_3$ at the range of temperature from 40 °C to 200 °C. (b) TGA curve of freshly prepared pyrim-UiO-68 (black) and pyrim-UiO-$IrCl_3$ (red) from 200-700 °C. The increased weight of metalated MOF is due to the presence of iridium within the MOF.

3.2 Synthesis of pyrim-UiO-IrH.

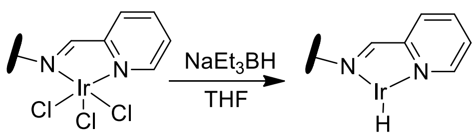

Pyrim-UiO-$IrCl_3$ (0.016 g, 0.0038 mmol) was charged into a vial containing 3 mL of THF. $NaEt_3BH$ (15 µL, 1 M in toluene) was added dropwise to the vial, and the mixture was stirred gently for 1 h at room temperature to give pyrim-UiO-IrH as black colored solid. The resultant MOF catalyst was separated via centrifugation and then washed with THF several times. Pyrim-UiO-IrH was then used directly for the catalysis.

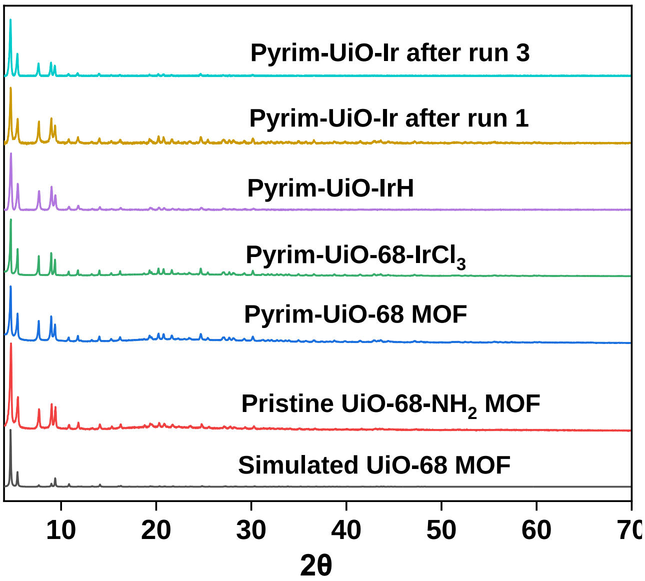

Figure S3. PXRD patterns of simulated UiO-68 MOF (black), pristine UiO-68-NH_2 MOF (red), pyrim-UiO-68 MOF (blue), pyrim-UiO-$IrCl_3$ (green), pyrim-UiO-IrH (violet), pyrim-UiO-Ir after run 1 (mustard brown) and pyrim-UiO-Ir after run 3 (light blue).

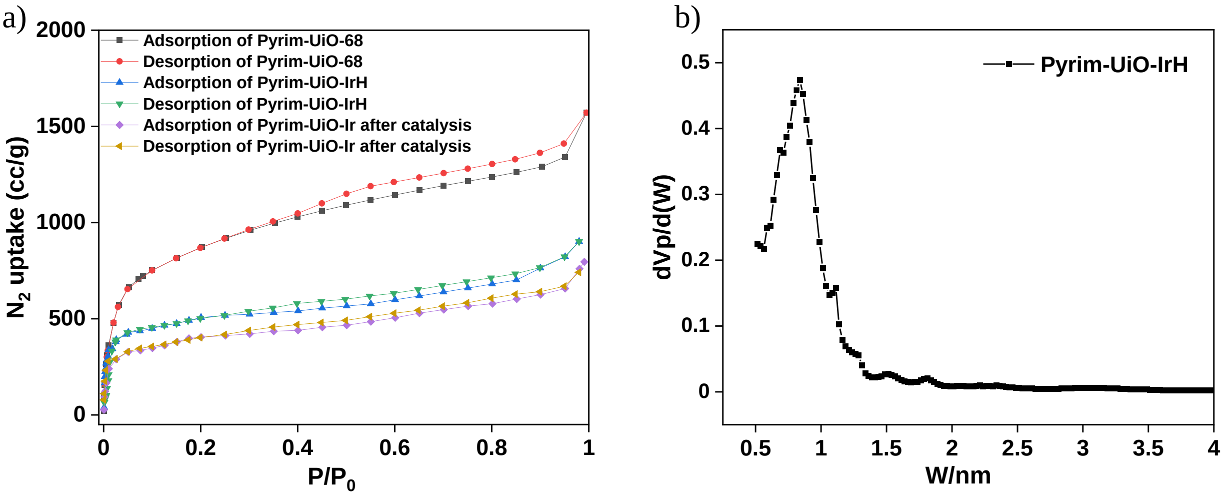

Figure S4. a) Brunauer−Emmett−Teller (BET) nitrogen sorption isotherms of pyrim-UiO-68, pyrim-UiO-IrH and pyrim-UiO-Ir after catalysis measured at 77 K. Pyrim-UiO-68 and pyrim-UiO-IrH have a BET surface area of 2342 m^2/g and 1245 m^2/g respectively. b) HK pore distribution plot of pyrim-UiO-IrH. Pore size for pyrim-UiO-IrH was determined to be 0.8 nm.

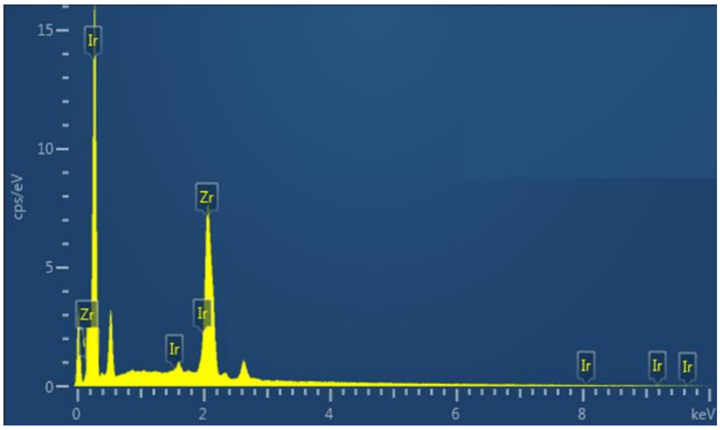

Figure S5. SEM-EDX analysis of pyrim-UiO-IrH.

3.3. Synthesis of homogeneous pyridylimine-iridium complex.

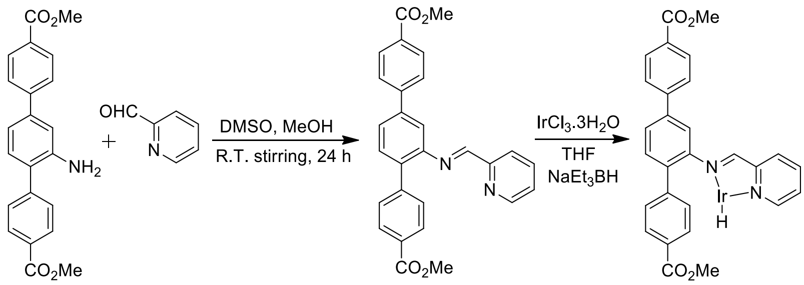

Under inert condition, dimethyl 2'-amino-[1,1':4',1"-terphenyl]-4,4"-dicarboxylate (0.200 g, 0.553 mmol) was dissolved in 30 mL of DMSO in a 50 mL Schlenk flask. To the reaction mixture, 1 mL of methanol was added followed by the addition of 2-pyridine carboxaldehyde (0.073 mL, 0.774 mmol). The resulting clear light-yellow colour solution was stirred for 24 h at room temperature. A light-yellow precipitate was formed, which was isolated through centrifugation followed by washing with methanol for three times and then dried under vacuum to afford the pyridylimine ligand as a yellow solid (0.180 g, 0.399 mmol, 72%). ^{1}H NMR (500 MHz, $CDCl_3$): δ 8.71 (s, 2 H), 8.14 (d, $^3J_{H-H}$ = 8.2 Hz, 2 H), 8.09 (s, 2 H), 8.02 (d, $^3J_{H-H}$ = 7.9 Hz, 1 H), 7.77 (dd, $^3J_{H-H}$ = 14.0, 8.2 Hz, 3 H), 7.66 – 7.58 (m, 4 H), 7.44 (s, 1 H), 7.40 – 7.36 (m, 1 H), 3.95 (d, $^3J_{H-H}$ = 6.8 Hz, 6 H). m/z (ESI) Anal calcd. for $C_{28}H_{23}N_2O_4[M+H]^+$: 451.1658; Found: 451.1641 (err. -3.7 ppm).

In a vial, the pyridylimine ligand, dimethyl 2'-((pyridin-2-ylmethylene)amino)-[1,1':4',1"-terphenyl]-4,4"-dicarboxylate (0.036 g, 0.080 mmol), was added to a solution of $IrCl_3.3H_2O$ (0.028 g, 0.080 mmol) in THF (until saturated). It was then left overnight, the pyridylimine-iridium complex was obtained. $NaEt_3BH$ (15 µL, 1 M in toluene) was added dropwise to the vial containing complex, and the mixture was stirred gently for 1 h at room temperature to give pyridylimine-iridium hydride complex.

4. Catalytic reactions with pyrim-UiO-IrH.

4.1. General procedure for pyrim-UiO-IrH catalysed borylation of methane.

$$CH_4 + B_2pin_2 \xrightarrow{\text{pyrim-MOF-IrH}} CH_3Bpin$$

In the glovebox, pyrim-UiO-IrH (0.5 mol% of Ir) in 2 mL solvent was transferred into a glass liner. B_2pin_2 was subsequently added to the liner, which was then securely fitted into a high-pressure reactor and sealed. The sealed Parr reactor was then removed from the glovebox and purged with CH_4 two to three times. Subsequently, the Parr reactor was pressurized to 20-40 bar with CH_4 and heated to a temperature range of 110-150 °C, where it was maintained for a duration of 10 to 48 hours. The reactor was subsequently cooled, and the pressure was released. The MOF was separated from the reaction mixture through centrifugation, and the resulting supernatant was analyzed using GC-MS and GC-FID to determine the conversion and yield for CH_3Bpin.

Table S1. Optimization reaction conditions for borylation of methane.[a]

$$CH_4 + B_2pin_2 \xrightarrow[\text{Solvent, Time, Pressure, Temp.}]{\text{Pyrim-UiO-IrH}} CH_3Bpin$$

Entry	Catalyst	Borylating agent	Temperature (°C)	Pressure (bar)	Time (h)	Solvent	%GC-Yield (Selectivity)
1	Pyrim-UiO-IrH (0.5 mol%)	B_2pin_2 (0.2 mmol)	130	40	12 h	CyH	54 (98)
2	Pyrim-UiO-IrH (0.5 mol%)	B_2pin_2 (0.2 mmol)	130	40	18 h	CyH	85 (98)
3	**Pyrim-UiO-IrH (0.5 mol%)**	**B_2pin_2 (0.2 mmol)**	**130**	**40**	**24 h**	**CyH**	**98 (98)**
4	Pyrim-UiO-IrH (0.5 mol%)	B_2pin_2 (0.2 mmol)	130	40	30 h	CyH	90 (90)
5	Pyrim-UiO-IrH (0.5 mol%)	B_2pin_2 (0.2 mmol)	130	40	48 h	CyH	82 (82)
6	Pyrim-UiO-IrH (0.5 mol%)	B_2pin_2 (0.2 mmol)	110	40	24 h	CyH	19 (95)
7[b]	Pyrim-UiO-IrH (0.5 mol%)	B_2pin_2 (0.2 mmol)	150	40	24 h	CyH	78 (78)
8	Pyrim-UiO-IrH (0.5 mol%)	B_2pin_2 (0.2 mmol)	130	20	24 h	CyH	26 (96)
9	Pyrim-UiO-IrH (0.5 mol%)	B_2pin_2 (0.2 mmol)	130	30	24 h	CyH	47 (98)

10	Pyrim-UiO-IrH (0.3 mol%)	B_2pin_2 (0.2 mmol)	130	40	24 h	CyH	30 (98)
11	Pyrim-UiO-IrH (0.5 mol%)	B_2pin_2 (0.2 mmol)	130	40	24 h	THF	29 (33)
12	Pyrim-UiO-IrH (0.5 mol%)	B_2pin_2 (0.2 mmol)	130	40	24 h	Toluene	35 (44)
13	Pyrim-UiO-IrH (0.5 mol%)	B_2pin_2 (0.2 mmol)	130	40	24 h	Heptane	72 (86)
14	Pyrim-UiO-IrH (0.5 mol%)	B_2pin_2 (0.2 mmol)	130	40	24 h	DMF	21 (24)
15	No catalyst	B_2pin_2 (0.2 mmol)	130	40	24 h	CyH	0
16	Pyrim-UiO-68	B_2pin_2 (0.2 mmol)	130	40	24 h	CyH	0
17	$IrCl_3.3H_2O$ (0.5 mol%)	B_2pin_2 (0.5 mmol)	130	40	24 h	CyH	0
18[c]	Pyrim-UiO-IrH (0.5 mol%)	HBpin (0.2 mmol)	130	40	24 h	CyH	0

[a]Reaction conditions: 1.9 mg of pyrim-UiO-IrH (1.02 μmol of Ir), 51 mg B_2pin_2 (0.2 mmol), 2 mL solvents. [b]Lower yield was due to the generation of sol-Bpin and oxygenated byproducts such as HOBpin and pinBOBpin, stemming from the interaction of B_2pin_2 with OH groups residing on the Zr_6 nodes of the MOF.[6,7] [c]HBpin was used as the borylating agent.

4.2. Blank reaction of pyrim-UiO-IrH with B_2pin_2 under N_2 without methane.

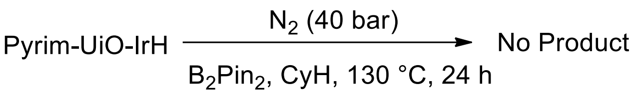

In the glovebox, pyrim-UiO-IrH (1.9 mg, 0.5 mol% of Ir) in 2 mL cyclohexane was transferred into a glass liner. B_2pin_2 (51 mg, 0.2 mmol) was subsequently added to the liner, which was then securely fitted into a high-pressure reactor and sealed. The sealed Parr reactor was then removed from the glovebox and purged with N_2 two to three times. The reactor was pressurized with 40 bar nitrogen and then heated at 130 °C for 24 h without any mechanical stirring. The reactor was subsequently cooled, and the pressure was released. The MOF was separated from the reaction mixture through centrifugation, and the resulting supernatant was analyzed using GC-MS and GC-FID to determine the conversion and yield for CH_3Bpin. In this reaction, no trace of products was formed, suggesting CH_4 as the sole carbon source for CH_3Bpin in the pyrim-UiO-IrH catalyzed methane borylation.

4.3. Test for "heterogeneity" of pyrim-UiO-IrH in borylation of CH_4.

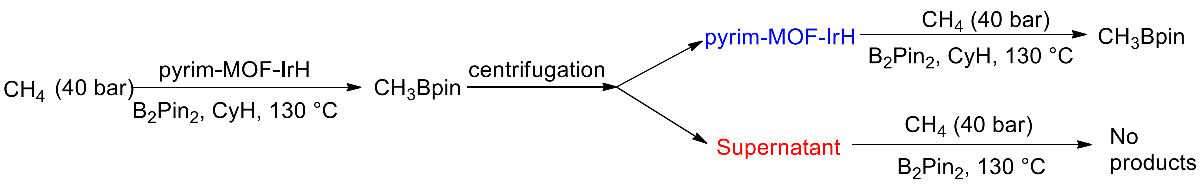

Figure S6. Heterogeneity test of pyrim-UiO-IrH for the borylation of methane.

In the glovebox, pyrim-UiO-IrH (1.9 mg, 0.5 mol% of Ir) in 2 mL cyclohexane was transferred into a glass liner. B_2pin_2 (51 mg, 0.2 mmol) was subsequently added to the liner, which was then securely fitted into a high-pressure reactor and sealed. The sealed Parr reactor was then removed from the glovebox and purged with CH_4 two to three times. The reactor was pressurized with 40 bar methane and then heated at 130 °C for 24 h without any mechanical stirring. The system was subsequently cooled, and the pressure was released. The solid MOF was removed from suspension to separate the solid and the supernatant, inside the glove box and washed with cyclohexane multiple times.

Two reactions were set up separately in two different Parr reactors, one with the solid and the other one with the supernatant recovered from the previous reaction. The extracted solid and supernatant were added into two separate liners, and B_2pin_2 (51 mg, 0.2 mmol) was added to each liner. 2 mL cyclohexane was added to the liner containing the solid MOF. Then both the liners were fitted into two separate Parr reactors and sealed. The sealed Parr reactors were taken out from the glovebox and purged with CH_4 gas two times. The Parr reactors were pressurized to 40 bar of CH_4 and stirred at 130°C for 24 h. After the completion of the reaction, the pressure of the reactors was released. The reactions were analysed with the GC-MS and GC-FID, which showed that the reaction with the solid MOF gave 98% yield, while the reaction with supernatant gave 0% conversion. This experiment excludes the potential of any leached Ir-species responsible for catalysis and confirms that solid pyrim-UiO-IrH was the actual catalyst for the borylation of methane.

4.4. Recycling of pyrim-UiO-IrH for the borylation of methane.

The recycle and reuse experiment was conducted at ~50-60% conversion to check the stability of the pyrim-UiO-IrH MOF-catalyst (Table S2). The detailed procedure of recycling experiment given below.

In the glovebox, pyrim-UiO-IrH (1.9 mg, 0.5 mol% of Ir) in 2 mL cyclohexane was transferred into a glass liner. B_2pin_2 (51 mg, 0.2 mmol) was subsequently added to the

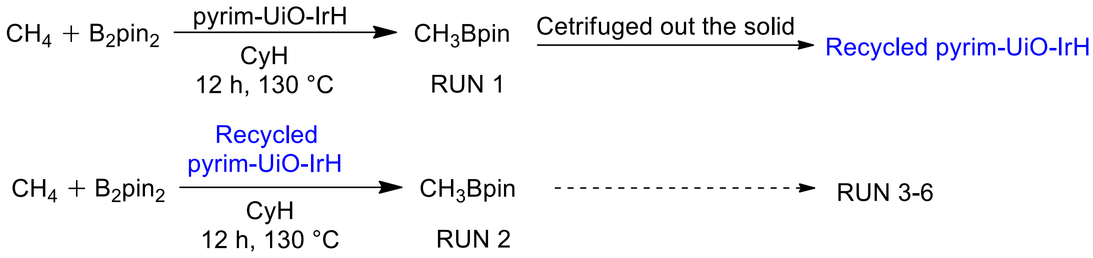

Figure S7. Recycle and reuse of pyrim-UiO-IrH in borylation of methane.

liner, which was then securely fitted into a high-pressure reactor and sealed. The sealed Parr reactor was then removed from the glovebox and purged with CH_4 two to three times. The reactor was pressurized with 40 bar methane and then heated at 130 °C for 12 h without any mechanical stirring. The system was subsequently cooled, and the pressure was released. The solid MOF was removed from suspension to separate the solid and the supernatant, inside the glove box and washed with cyclohexane multiple times. The yield of CH_3Bpin was determined by GC-MS and GC-FID analysis. The solid MOF was then recycled.

Inside the glovebox, the recovered MOF-catalyst was again added to the glass liner. 2 mL cyclohexane and B_2pin$_2$ (51 mg, 0.2 mmol) were added to the glass liner and sealed it in a Parr reactor. The Parr reactor was taken out from the glove box and was purged with the CH_4 gas and then pressurized it to 40 bar of CH_4. The reactor was heated at 130 °C for 12 h. After the reaction, the solution was analyzed in the same way as mentioned previously in run 1. The recycling and reuse experiments were performed up to 5 times in total.

Table S2. %Conversion of B_2pin$_2$, %GC-Yield of CH_3Bpin and the leaching of Ir and Zr at various runs of the recycling of pyrim-UiO-IrH in the borylation of methane.

Run	Time	%Conv. (B_2pin$_2$)	%GC-Yield	%Leaching (Ir, Zr)
Run-1	12 h	56	55	0.013, 0.03
Run-2	12 h	55	54	
Run-3	12 h	59	58	0.04, 0.06
Run-4	12 h	53	51	
Run-5	12 h	54	52	0.06, 0.08
Run-6	12 h	53	50	

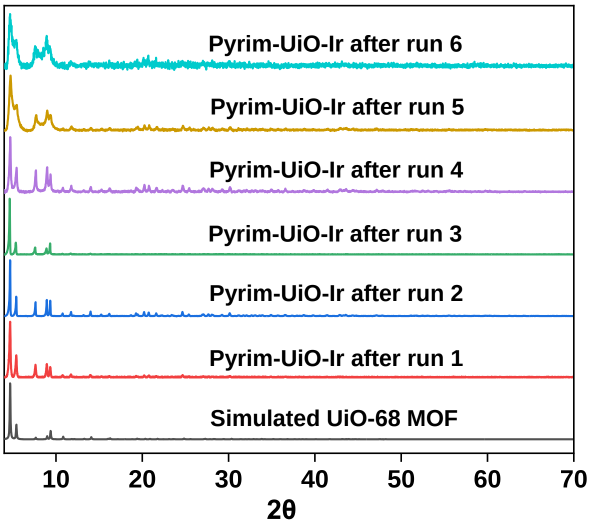

Figure S8. PXRD patterns of simulated UiO-68 MOF (black), pyrim-UiO-Ir after run 1 (red), pyrim-UiO-Ir after run 2 (blue), pyrim-UiO-Ir after run 3 (green), pyrim-UiO-Ir after run 4 (violet), pyrim-UiO-Ir after run 5 (mustard brown) and pyrim-UiO-Ir after run 6 (light blue).

4.5. Investigation of the effect of pore sizes on the rate of catalysis. The effect of pore sizes on the rate of catalytic reaction was investigated by comparing the rate of borylation reactions of methane catalyzed by pyrim-UiO-IrH with that of pyrim-UiO-66-IrH under identical reaction conditions. Pyrim-UiO-66-IrH has the same topology but smaller pore sizes compared to pyrim-UiO-IrH.

4.5.1 Synthesis and characterizations of pyrim-UiO-66-IrH. The synthesis was performed following a modified procedure.[8] In a vial, 2- aminoterephthalic acid (0.032 g, 0.176 mmol) was dissolved in a DMF solution (4.5 mL) followed by the addition of $ZrCl_4$ (0.044 g, 0.188 mmol). The mixture was sonicated for 20 minutes and then placed in a teflon sealed hydro bomb and heated at 120 °C for 24 h. After cooling to room temperature, the crystalline solids were isolated by centrifugation and washed by DMF several times to afford UiO-66-NH_2 MOF. UiO-66-NH_2-MOF was functionalized with pyridylimine moiety. In a 1.5 mL centrifuge tube, UiO-66-NH_2 MOF (0.017 g, 0.016 mmol) was added in 1 mL DMF followed by addition of 2-pyridinecarboxaldehyde (6 µL, 0.056 mmol). It was then left overnight with periodic shaking. The solid was washed various times with DMF to obtain pyrim-UiO-66 as light brown solid. Pyrim-UiO-66 MOF (0.020 g, 0.009 mmol) in THF was charged into a vial, and then 1 mL THF solution of $IrCl_3.3H_2O$ (0.019 g, 0.054 mmol) was added to it. The mixture was stirred slowly overnight at room temperature. The resultant solid was centrifuged out of suspension and washed with THF 4-5 times. Pyrim-UiO-66-$IrCl_3$ has 28% Ir-loading based on ICP-OES analysis. Treatment of $NaEt_3BH$ (15 µL, 1 M in toluene) to pyrim-UiO-66-$IrCl_3$ (0.012 g, 0.00369 mmol) gave pyrim-UiO-66-IrH as black colored solid.

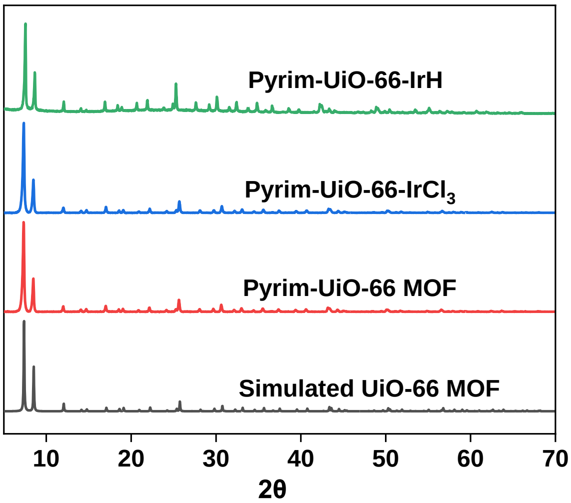

Figure S9. PXRD patterns of simulated UiO-66 MOF (black), pyrim-UiO-66 MOF (red), pyrim-UiO-66-$IrCl_3$ (blue) and pyrim-UiO-66-IrH (green).

4.5.2 Comparison of the catalytic activities of pyrim-UiO-IrH with that of pyrim-UiO-66-IrH in the borylation of methane under identical conditions.

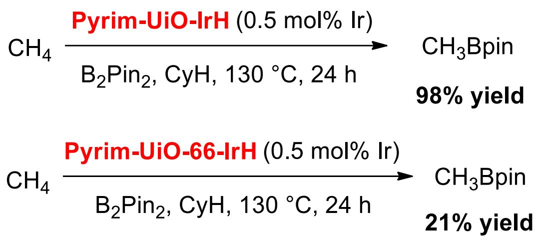

Figure S10. The borylation of methane catalyzed by pyrim-UiO-IrH with that of pyrim-UiO-66-IrH under identical reaction conditions.

In a glovebox, two separate 5 mL vials were charged with pre-activated pyrim-UiO-IrH (1.9 mg, 0.5 mol% of Ir) and pyrim-UiO-66-IrH (1.6 mg, 0.5 mol% of Ir) each and washed with THF multiple times. Each MOF slurry in 2 mL cyclohexane were transferred to two different glass liners containing B_2pin_2 (51 mg, 0.2 mmol). The liners were fitted into the Parr reactors and sealed properly. The sealed Parr reactors were taken out from the glove box. The reactors were purged twice with the CH_4, then charged with 40 bar CH_4 each and stirred at 130 °C for 24 h. After the completion of the reaction, the pressure from the reactors were released. The solid MOF was then removed from suspension inside the glove box and the supernatant were analysed by GC-MS. The yield of CH_3Bpin were 98% and 21% with pyrim-UiO-IrH and pyrim-UiO-66-IrH respectively. This experiment indicates that the larger pore size MOF (pyrim-UiO-IrH) have comparatively higher effieciency than the smaller pore size pyrim-UiO-66-IrH MOF due to the facile diffusion of substrates into the larger pores of pyrim-UiO-IrH.

4.6. C−H borylation of methane using pyrim-MOF-IrH and its homogeneous control [Ph(pyrim)(PhCO$_2$Me)$_2$]IrH as catalysts under identical conditions to compare their catalytic activities.

Out of the two Parr reactors, one was charged with B$_2$pin$_2$ (51 mg, 0.2 mmol), [Ph(pyrim)(PhCO$_2$Me)$_2$]IrH (0.0007 g, 0.0011 mmol) and cyclohexane (2 mL) and another reactor was charged with B$_2$pin$_2$ (51 mg, 0.2 mmol), pyrim-UiO-IrH (1.9 mg, 0.5 mol% Ir) and cyclohexane (2 mL) in a glovebox. Both the reactors were purged twice with CH$_4$, then charged with 40 bar CH$_4$ each and stirred at 130 °C for 24 h. After the completion of the reaction, the pressure from the reactors were released. The yield (%) of the products were monitored by GC-MS and GC-FID (Figure S11).

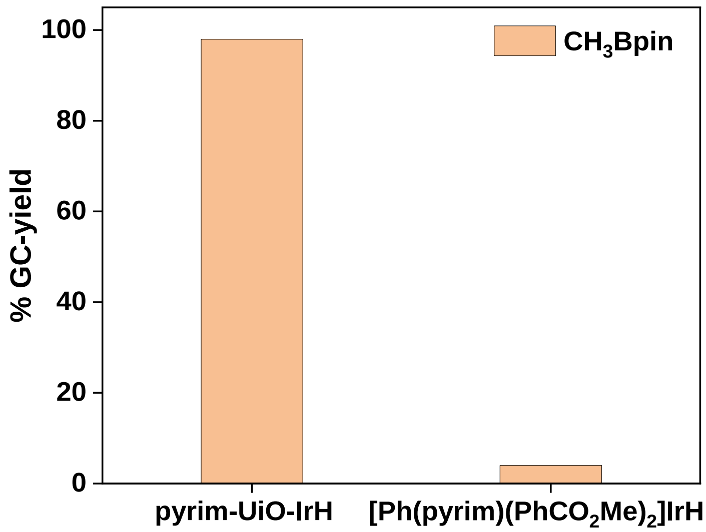

Figure S11. C−H borylation of methane using pyrim-UiO-IrH and its homogeneous control [Ph(pyrim)(PhCO$_2$Me)$_2$]IrH as catalysts under identical conditions.

Table S3. Comparison of pyrim-UiO-IrH with its homogeneous control [Ph(pyrim)(PhCO$_2$Me)$_2$]IrH in the borylation of methane under similar condition.

Catalyst	Ir (µmol)	Conv. of B$_2$Pin$_2$ (%)	CH$_3$Bpin (%)	CH$_2$(Bpin)$_2$ (%)	HBpin (%)	HOBpin (%)	solvBpin (%)	TON
Pyrim-UiO-IrH	1.02	100	98	0	0	1	1	196
[Ph(pyrim)(PhCO$_2$Me)$_2$]IrH	1.1	11	4	1	0	5	1	8

Reaction conditions: 2 mL of C$_6$H$_{12}$, 51 mg B$_2$pin$_2$ (0.2 mmol), 130 °C, 40 bar CH$_4$ and 24 h.

5. Analysis and quantification of CH_3Bpin by GC-MS and GC-FID.

A) The conversions and yields of the reactions were determined by Agilent 7890B gas chromatograph equipped with a flame ionisation detector (FID) and a mass detector (Agilent 5977B GC/MSD) and a HP-5MS Ultra Inert 30m-250μm-0.25μm column. GC conditions: Inj: 220 °C; Det: 250 °C; Column temp: 40 °C followed by a ramp of 5 °C/min to 240 °C; Column flow: 1.0 mL/min.

The conversion and yield of CH_3Bpin were determined for each reaction run by measuring the relative amount of boron species through the corrected integration of GC-MS peaks as follows.[7]

$$\text{Conversion\%} = \left[1 - \frac{B_2Pin_2 \text{ remaining}}{(B_2Pin_2 + CH_3Bpin + HOBpin + SolBpin + etc)}\right] \times 100\%$$

$$\text{Yield of } CH_3Bpin\% = \left[\frac{CH_3BPin}{(B_2Pin_2 + CH_3Bpin + HOBpin + SolBpin + etc)}\right] \times 100\%$$

$$\text{Selectivity of } CH_3Bpin\% = \left[\frac{CH_3Bpin}{\text{Overall product formed}}\right] \times 100\%$$

$$\text{TON of } CH_3Bpin = \frac{\%\text{ Yield of } CH_3Bpin}{\%\text{ Ir Loading}}$$

a)

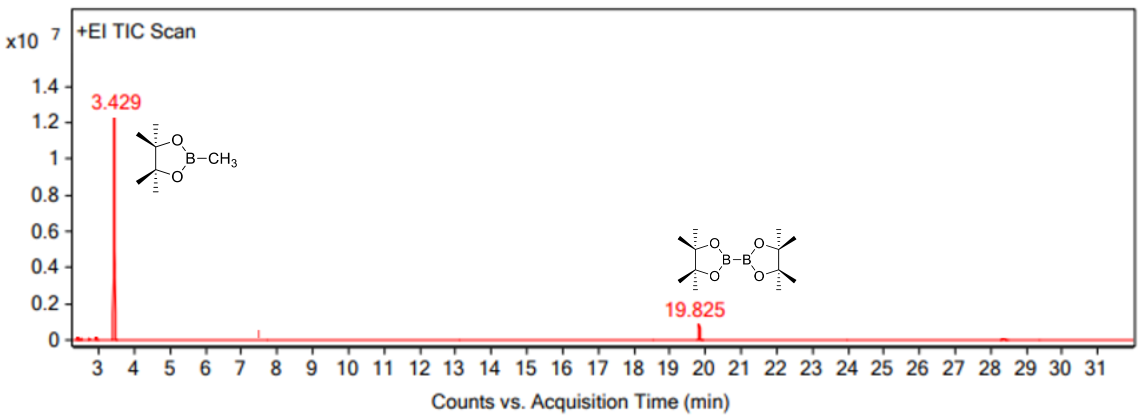

b)

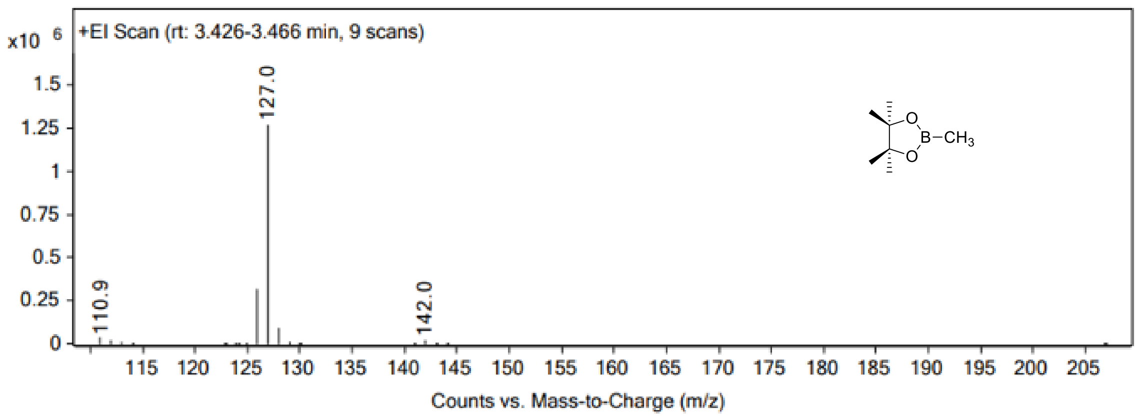

c)

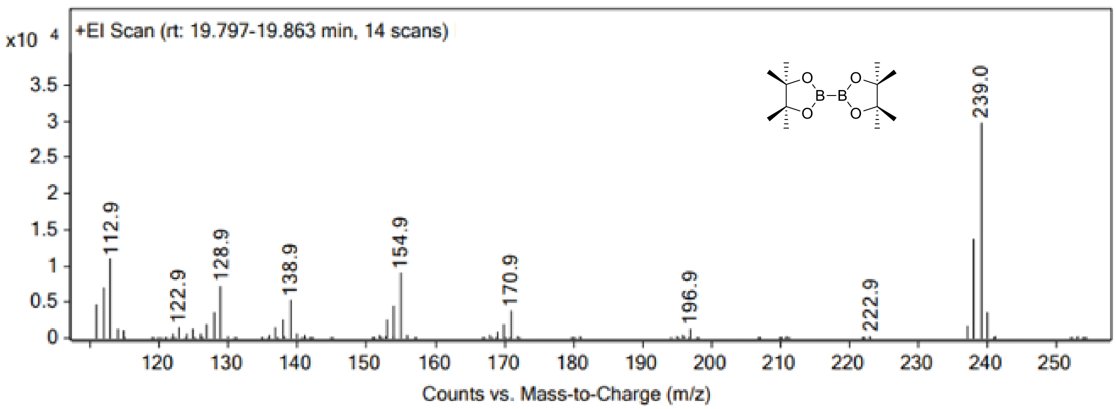

Figure S12. The GC-MS spectra of the crude reaction mixture after 18 h of catalysis (87% B_2pin_2 conversion) using pyrim-UiO-IrH. Reaction conditions: 1.9 mg of pyrim-UiO-IrH (1.02 μmol of Ir), 2 mL of C_6H_{12}, 51 mg B_2pin_2 (0.2 mmol), 130 °C, 40 bar CH_4 and 18 h.

a)

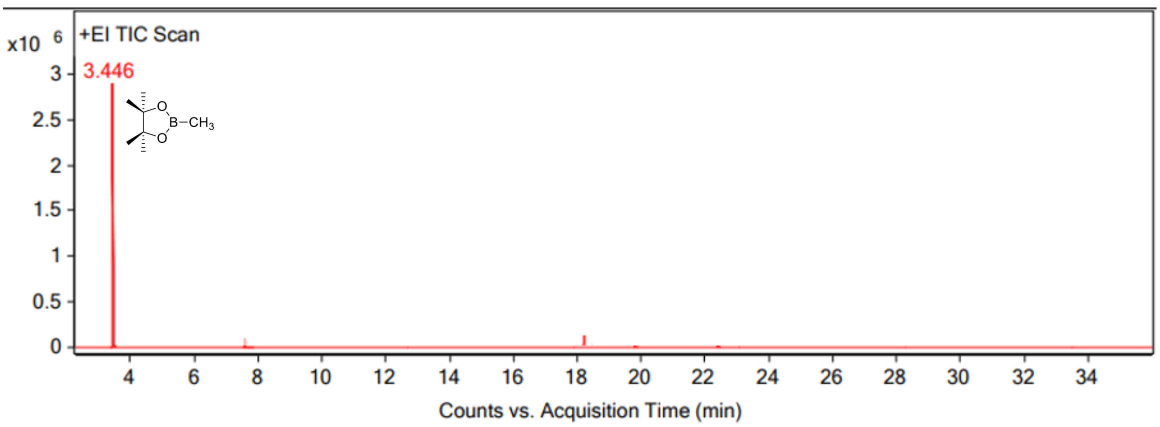

b)

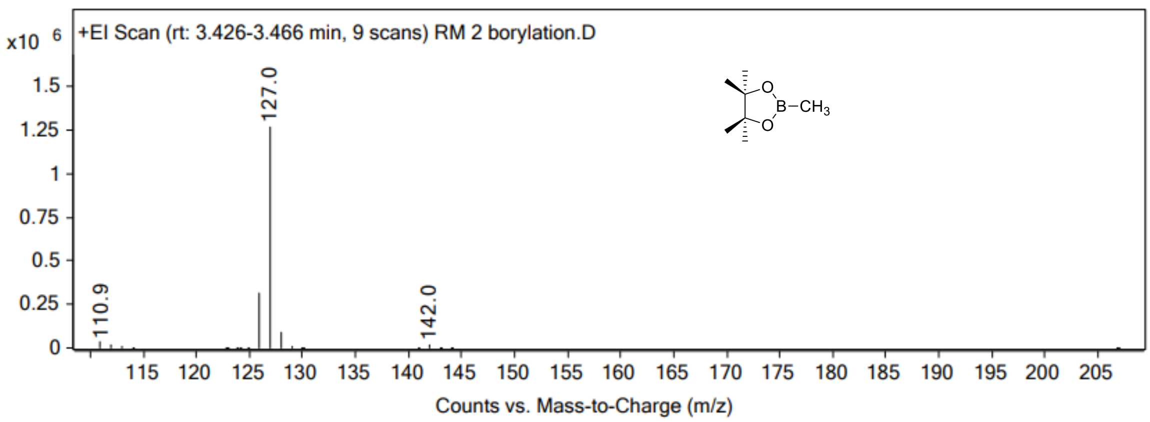

Figure S13. The GC-MS spectra of the crude reaction mixture after 24 h of catalysis (100% B_2pin_2 conversion) using pyrim-UiO-IrH. Reaction conditions: 1.9 mg of pyrim-UiO-IrH (1.02 μmol of Ir), 2 mL of C_6H_{12}, 51 mg B_2pin_2 (0.2 mmol), 130 °C, 40 bar CH_4 and 24 h.

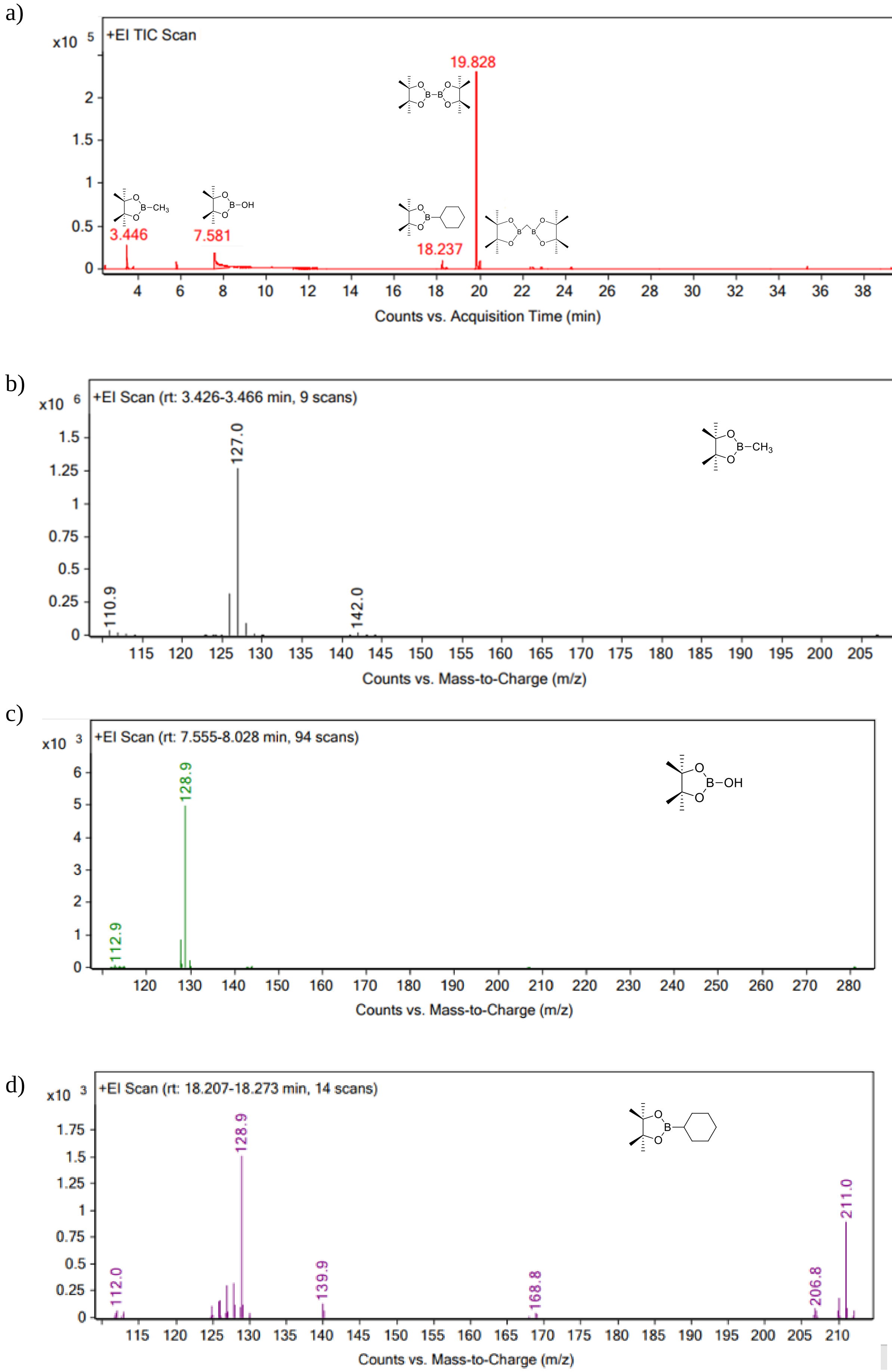
a)
x10 5
+EI TIC Scan
19.828
3.446
7.581
18.237
Counts vs. Acquisition Time (min)
b)
x10 6
+EI Scan (rt: 3.426-3.466 min, 9 scans)
127.0
110.9
142.0
Counts vs. Mass-to-Charge (m/z)
c)
x10 3
+EI Scan (rt: 7.555-8.028 min, 94 scans)
128.9
112.9
Counts vs. Mass-to-Charge (m/z)
d)
x10 3
+EI Scan (rt: 18.207-18.273 min, 14 scans)
128.9
112.0
139.9
168.8
206.8
211.0
Counts vs. Mass-to-Charge (m/z)

e)

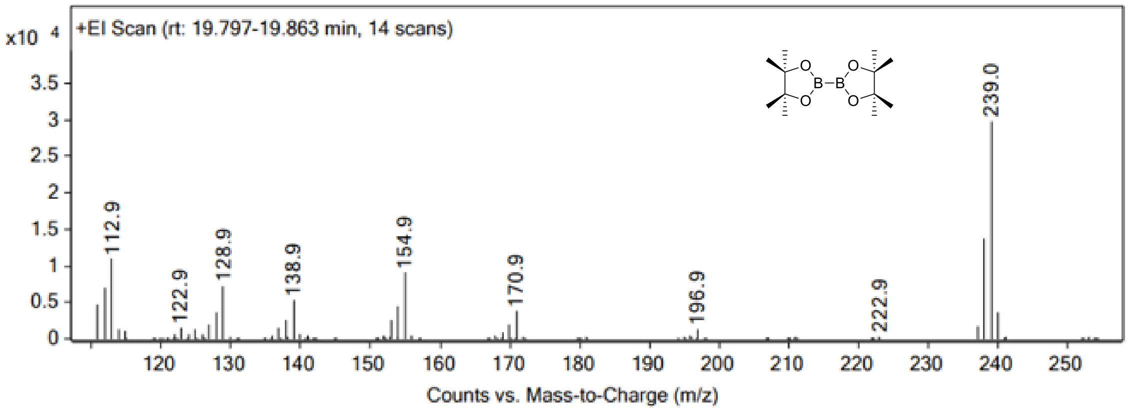

f)

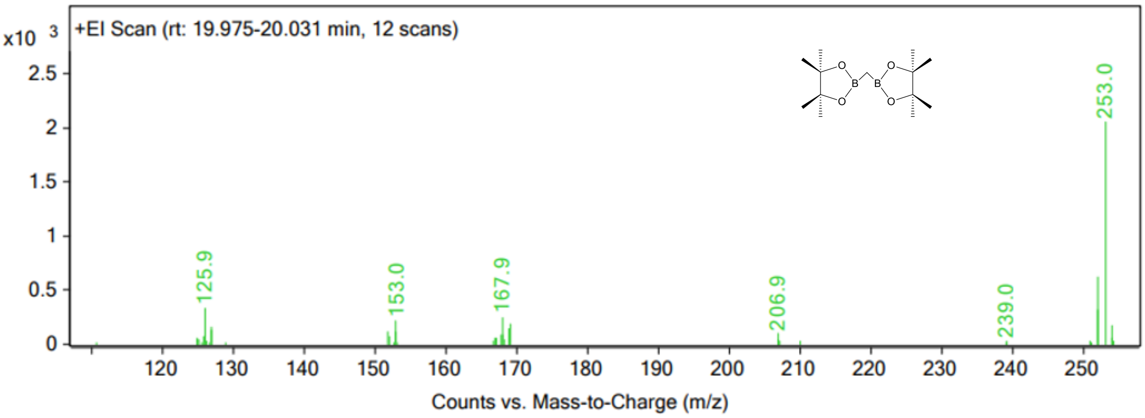

Figure S14. The GC-MS spectra of the crude reaction mixture after 24 h of catalysis (11% B_2pin_2 conversion) using [Ph(pyrim)($PhCO_2Me$)$_2$]IrH as the homogeneous control. Reaction conditions 0.0007 g of [Ph(pyrim)($PhCO_2Me$)$_2$]IrH (1.1 μmol of Ir), 2 mL of C_6H_{12}, 51 mg B_2pin_2 (0.2 mmol), 130 °C, 40 bar CH_4 and 24 h.

B) The yield of CH_3Bpin under optimized conditions [1.02 μmol of Ir, B_2pin_2 (0.2 mmol), 2 mL C_6H_{12}, 130 °C, 40 bar CH_4 and 24 h] was also determined by GC analysis using mesitylene as an internal standard. First, we made a GC-calibration curve using known quantities of MeBpin with mesitylene as an internal standard (I.S.) as shown below.

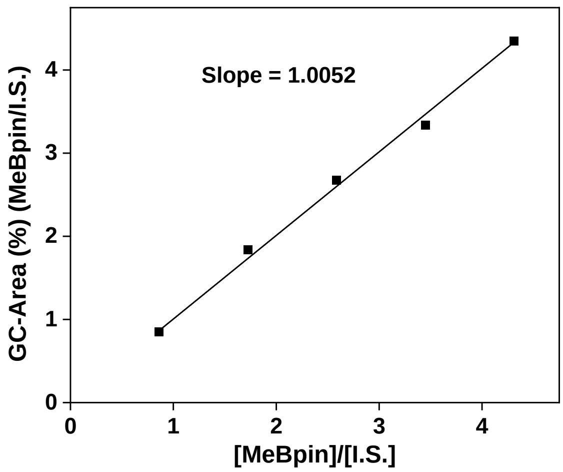

Figure S15. GC calibration plot employing various concentrations of MeBpin with mesitylene as an internal standard.

From the above calibration plot, slope = 1.0052

Analysis: [Mesitylene] = 0.07188618 M

%GC-Area of MeBpin peak = 57.68%

%GC-Area of Mesitylene peak = 42.32%

[MeBpin] =?

Now,

%GC-Area of MeBpin / %GC-Area of I.S. = Slope × [MeBpin] / [I.S.]

⇒ 57.68 / 42.32 = 1.0052 × [MeBpin] / 0.07188618

⇒ [MeBpin] = 0.0975 M

M = n / V

n (mmol) = M × V (mL)

mmol of MeBpin produced = 0.0975 × 2 = 0.195 mmol [Since 2 mL of solvent was used]

% Yield (MeBpin) = mmol of product (MeBpin)/ mmol of reactant taken × 100 %

= (0.195/0.2) × 100 = 97.5%

(The absence of a peak corresponding to B_2pin_2 in the GC spectrum indicates complete consumption of the reactant, signifying a full conversion rate)

The yields of MeBpin obtained using the GC-calibration curve is close to the value afforded from the alternative method described in above section 5A (SI), thereby confirming the reliability of our experimental protocol.

6. DFT calculations. All quantum chemical calculations were done using the density functional theory (DFT) functional B3LYP/genecp along with sdd basis set method for Ir and 6-31G basis set for C, N, H, O and B atoms as implemented in the Gaussian 16 software suite.[9–13] Electronic structure complexes were optimized at the unrestricted level. All calculations were performed in the solvated state and at 403.15 K. We used the Polarizable Continuum Model (PCM) using the integral equation formalism variant (IEFPCM) as the default SCRF method by using THF as the solvent for pyrim-UiO-$IrCl_3$(THF) at room temperature (298.15K) and cyclohexane as the solvent for all other molecules in this DFT calculation at 403.15 K. Each structure was first optimized, and then frequency calculation was performed to confirm its geometry and to obtain the thermochemical data.

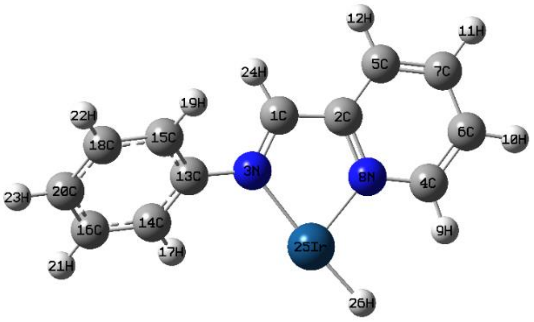

Pyrim-UiO-IrH

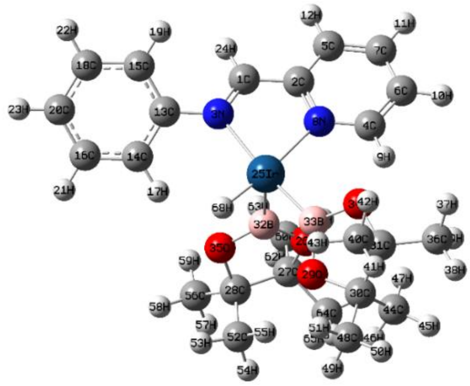

INT-1

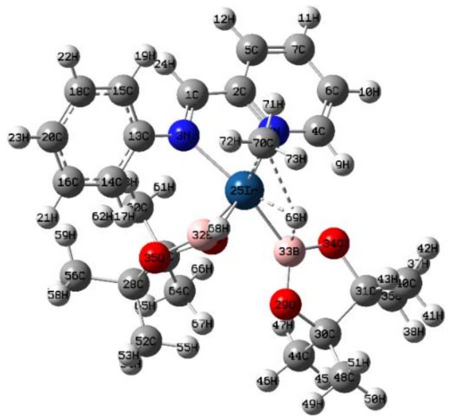

TS-1

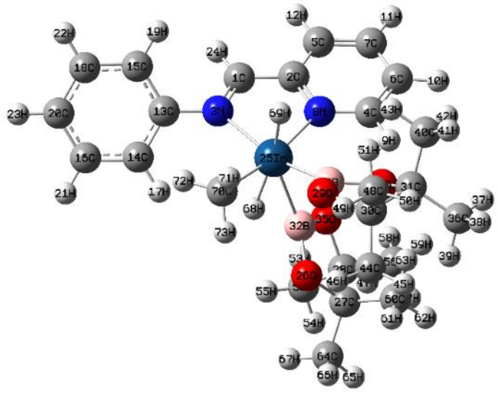

INT-2

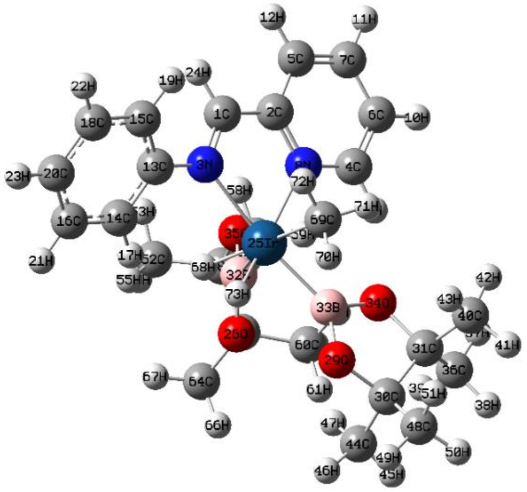

INT-3

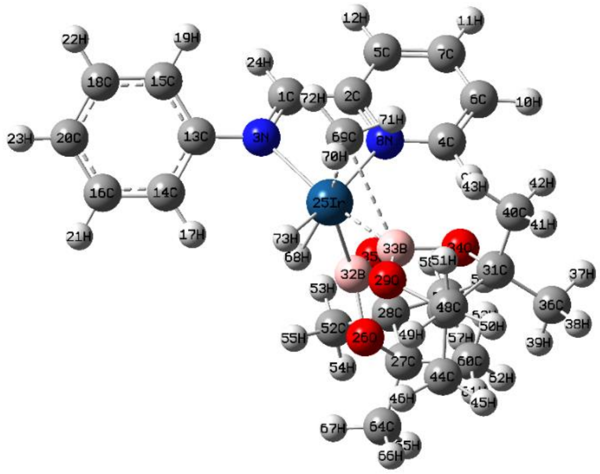

TS-2

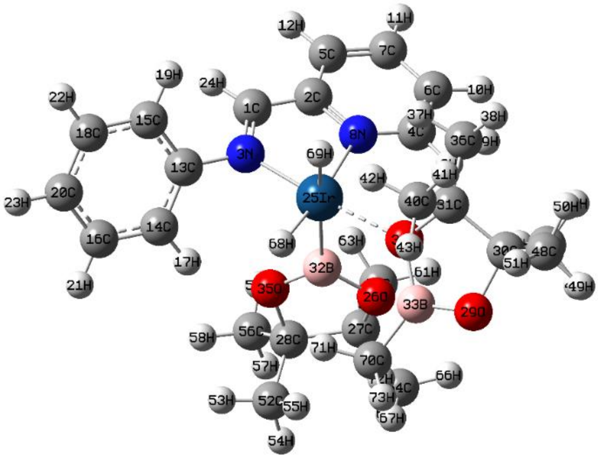

INT-4

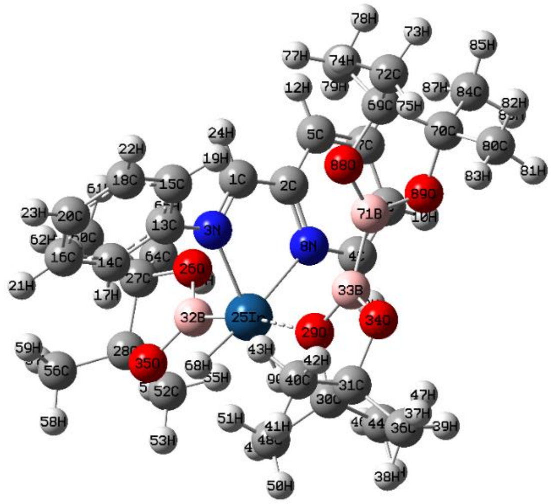

INT-5

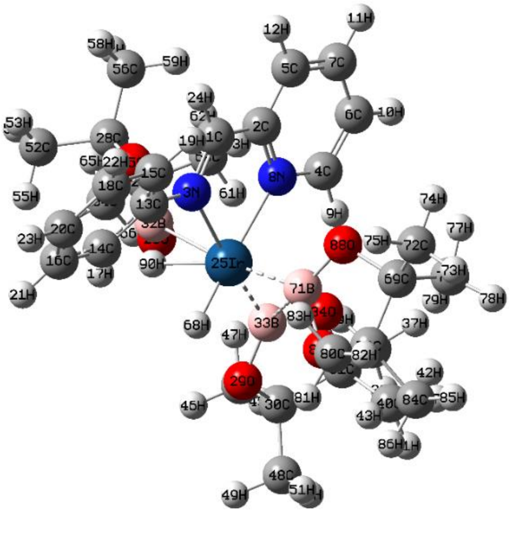

TS-3

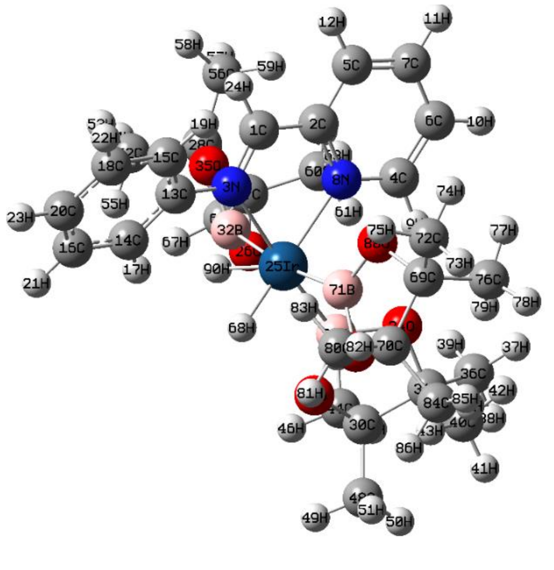

INT-6

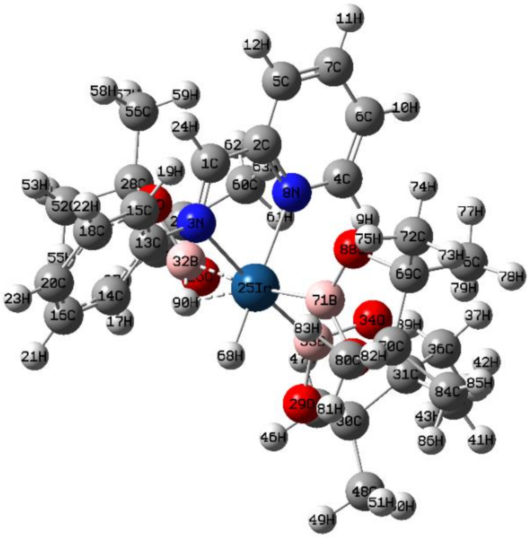

TS-4

Figure S16. DFT-optimized structures of intermediates and transition states of the catalytic cycle in pyrim-UiO-IrH catalysed methane borylation using B_2pin_2.

6.1. Cartesian coordinates of the DFT-optimized structures.

Cartesian coordinates of Pyrim-UiO-IrH

		Coordinates (Angstroms)		
S.No.	Atoms	X	Y	Z
1	C	-14.186325	-5.662331	-12.600542
2	C	-13.696708	-4.661369	-11.705306
3	N	-14.333675	-5.282408	-13.858102
4	C	-12.955394	-2.410745	-11.535603
5	C	-13.480725	-4.847629	-10.331602
6	C	-12.732818	-2.568860	-10.174692
7	C	-12.997000	-3.802325	-9.552443
8	N	-13.435550	-3.430502	-12.316832
9	H	-12.765836	-1.481978	-12.050312
10	H	-12.355178	-1.728139	-9.605455
11	H	-12.827447	-3.934828	-8.490954
12	H	-13.698262	-5.817356	-9.898437
13	C	-14.758960	-6.206432	-14.862166
14	C	-15.608466	-5.740958	-15.880226
15	C	-14.322602	-7.543773	-14.871096
16	C	-16.032715	-6.610653	-16.888433
17	H	-15.940581	-4.707588	-15.856861
18	C	-14.745689	-8.404998	-15.887911
19	H	-13.634676	-7.895579	-14.109833
20	C	-15.602640	-7.944369	-16.896365
21	H	-16.696151	-6.247364	-17.666089
22	H	-14.397810	-9.432588	-15.897680
23	H	-15.925215	-8.615935	-17.684823
24	H	-14.434135	-6.660362	-12.254966
25	Ir	-13.784312	-3.294161	-14.232310
26	H	-13.286125	-1.725904	-14.413264

Cartesian coordinates of INT-1

		Coordinates (Angstroms)		
S.No.	Atoms	X	Y	Z
1	C	-13.876811	-5.699012	-12.934968
2	C	-13.062349	-4.846612	-12.083608
3	N	-14.209485	-5.306337	-14.130494
4	C	-11.902242	-2.816219	-11.888750
5	C	-12.744079	-5.197099	-10.765923
6	C	-11.558690	-3.112052	-10.563518
7	C	-11.981147	-4.316503	-9.993501
8	N	-12.640894	-3.666922	-12.638150
9	H	-11.594864	-1.906946	-12.393919
10	H	-10.966725	-2.403644	-9.996265
11	H	-11.724638	-4.565721	-8.970076
12	H	-13.094687	-6.139040	-10.358910
13	C	-15.000907	-6.175041	-14.953397
14	C	-16.098188	-5.633963	-15.641170
15	C	-14.692169	-7.541861	-15.066029
16	C	-16.902449	-6.477626	-16.412592
17	H	-16.306389	-4.574304	-15.539318
18	C	-15.491858	-8.369878	-15.860043
19	H	-13.815083	-7.942651	-14.567863
20	C	-16.603460	-7.842637	-16.527805
21	H	-17.762030	-6.065834	-16.931431
22	H	-15.241799	-9.421003	-15.961142
23	H	-17.225335	-8.486919	-17.140834
24	H	-14.224532	-6.650760	-12.533004
25	Ir	-13.285015	-3.339631	-14.783555
26	O	-14.832899	-0.725751	-14.297569
27	C	-16.197391	-0.269809	-13.892823
28	C	-17.116161	-1.394715	-14.506358
29	O	-11.951421	-0.996241	-16.412322
30	C	-11.269160	0.312018	-16.188780
31	C	-10.545731	0.070442	-14.811240
32	B	-14.847362	-2.125970	-14.538091
33	B	-12.190573	-1.648481	-15.169758
34	O	-11.435215	-0.944031	-14.172203
35	O	-16.200161	-2.579081	-14.490704
36	C	-10.474592	1.287124	-13.890054
37	H	-9.987051	1.009377	-12.949474
38	H	-9.888332	2.091575	-14.350573
39	H	-11.471126	1.667165	-13.657462
40	C	-9.165260	-0.588137	-14.952217
41	H	-8.426445	0.107866	-15.364732
42	H	-8.821157	-0.907870	-13.963395

43	H	-9.214906	-1.469558	-15.598493
44	C	-12.380138	1.369731	-16.119575
45	H	-11.970481	2.376970	-15.982518
46	H	-12.941161	1.348649	-17.058936
47	H	-13.078361	1.145885	-15.308951
48	C	-10.339933	0.576127	-17.372433
49	H	-10.935012	0.688271	-18.284254
50	H	-9.770841	1.501811	-17.222287
51	H	-9.638232	-0.246485	-17.526073
52	C	-17.483657	-1.147543	-15.975516
53	H	-17.988735	-2.036287	-16.366923
54	H	-18.162728	-0.293916	-16.079341
55	H	-16.589296	-0.979634	-16.580536
56	C	-18.354557	-1.743896	-13.683776
57	H	-19.031598	-0.883598	-13.616881
58	H	-18.894978	-2.563584	-14.167774
59	H	-18.091073	-2.062280	-12.672882
60	C	-16.207784	-0.241773	-12.357918
61	H	-15.398536	0.408633	-12.012465
62	H	-17.155310	0.147053	-11.968672
63	H	-16.042851	-1.241297	-11.944083
64	C	-16.415794	1.130057	-14.462201
65	H	-17.434459	1.480397	-14.256024
66	H	-15.714832	1.829003	-13.994687
67	H	-16.246900	1.150162	-15.540468
68	H	-13.608677	-3.338509	-16.309609

Cartesian coordinates of TS-1

		Coordinates (Angstroms)		
S.No.	Atoms	X	Y	Z
1	C	-13.831763	-5.735345	-12.948223
2	C	-13.017301	-4.882945	-12.096864
3	N	-14.164436	-5.342670	-14.143750
4	C	-11.857193	-2.852553	-11.902006
5	C	-12.699030	-5.233432	-10.779179
6	C	-11.513641	-3.148385	-10.576774
7	C	-11.936098	-4.352836	-10.006756
8	N	-12.595845	-3.703255	-12.651405
9	H	-11.549815	-1.943279	-12.407175
10	H	-10.921676	-2.439977	-10.009520
11	H	-11.679589	-4.602054	-8.983331
12	H	-13.049638	-6.175373	-10.372165
13	C	-14.955859	-6.211374	-14.966652
14	C	-16.053139	-5.670296	-15.654425
15	C	-14.647120	-7.578195	-15.079285
16	C	-16.857401	-6.513959	-16.425847
17	H	-16.261340	-4.610637	-15.552573
18	C	-15.446810	-8.406211	-15.873298
19	H	-13.770035	-7.978984	-14.581118
20	C	-16.558411	-7.878970	-16.541060
21	H	-17.716982	-6.102167	-16.944686
22	H	-15.196750	-9.457336	-15.974397
23	H	-17.180286	-8.523252	-17.154089
24	H	-14.179483	-6.687093	-12.546259
25	Ir	-13.239966	-3.375964	-14.796810
26	O	-14.787851	-0.762084	-14.310824
27	C	-16.152342	-0.306142	-13.906078
28	C	-17.071112	-1.431048	-14.519613
29	O	-11.906373	-1.032574	-16.425577
30	C	-11.224111	0.275685	-16.202036
31	C	-10.500682	0.034109	-14.824496
32	B	-14.802314	-2.162303	-14.551346
33	B	-12.145524	-1.684814	-15.183014
34	O	-11.390167	-0.980364	-14.185459
35	O	-16.155113	-2.615415	-14.503959
36	C	-10.429543	1.250791	-13.903310
37	H	-9.942002	0.973044	-12.962729
38	H	-9.843283	2.055242	-14.363828
39	H	-11.426078	1.630832	-13.670718
40	C	-9.120211	-0.624470	-14.965472
41	H	-8.381396	0.071533	-15.377987
42	H	-8.776108	-0.944203	-13.976650
43	H	-9.169857	-1.505892	-15.611748
44	C	-12.335090	1.333398	-16.132830
45	H	-11.925432	2.340637	-15.995774
46	H	-12.896113	1.312316	-17.072191
47	H	-13.033312	1.109552	-15.322206
48	C	-10.294884	0.539794	-17.385688
49	H	-10.889963	0.651938	-18.297509
50	H	-9.725792	1.465478	-17.235542
51	H	-9.593183	-0.282818	-17.539329
52	C	-17.438608	-1.183876	-15.988771
53	H	-17.943686	-2.072620	-16.380178
54	H	-18.117679	-0.330249	-16.092597
55	H	-16.544247	-1.015967	-16.593791
56	C	-18.309508	-1.780229	-13.697032
57	H	-18.986550	-0.919931	-13.630136
58	H	-18.849930	-2.599917	-14.181029
59	H	-18.046024	-2.098613	-12.686137
60	C	-16.162736	-0.278106	-12.371173
61	H	-15.353487	0.372300	-12.025720
62	H	-17.110262	0.110720	-11.981927
63	H	-15.997802	-1.277630	-11.957339
64	C	-16.370745	1.093724	-14.475457
65	H	-17.389410	1.444064	-14.269279
66	H	-15.669783	1.792670	-14.007942
67	H	-16.201851	1.113829	-15.553723
68	H	-13.842928	-3.061514	-16.200790
69	H	-11.795354	-3.881995	-15.097857
70	C	-13.273335	-4.877812	-16.162182
71	H	-12.964560	-5.790262	-15.696356
72	H	-14.266464	-4.990619	-16.544110
73	H	-12.606569	-4.644169	-16.965757

Cartesian coordinates of INT-2

		Coordinates (Angstroms)		
S.No.	Atoms	X	Y	Z
1	C	-13.831763	-5.735345	-12.948223
2	C	-13.017301	-4.882945	-12.096864
3	N	-14.164436	-5.342670	-14.143750
4	C	-11.857193	-2.852553	-11.902006
5	C	-12.699030	-5.233432	-10.779179
6	C	-11.513641	-3.148385	-10.576774
7	C	-11.936098	-4.352836	-10.006756
8	N	-12.595845	-3.703255	-12.651405
9	H	-11.549815	-1.943279	-12.407175
10	H	-10.921676	-2.439977	-10.009520
11	H	-11.679589	-4.602054	-8.983331
12	H	-13.049638	-6.175373	-10.372165
13	C	-14.955859	-6.211374	-14.966652
14	C	-16.053139	-5.670296	-15.654425
15	C	-14.647120	-7.578195	-15.079285
16	C	-16.857401	-6.513959	-16.425847
17	H	-16.261340	-4.610637	-15.552573
18	C	-15.446810	-8.406211	-15.873298
19	H	-13.770035	-7.978984	-14.581118
20	C	-16.558411	-7.878970	-16.541060
21	H	-17.716982	-6.102167	-16.944686
22	H	-15.196750	-9.457336	-15.974397
23	H	-17.180286	-8.523252	-17.154089
24	H	-14.179483	-6.687093	-12.546259
25	Ir	-13.239966	-3.375964	-14.796810
26	O	-14.787851	-0.762084	-14.310824
27	C	-16.152342	-0.306142	-13.906078
28	C	-17.071112	-1.431048	-14.519613
29	O	-11.906373	-1.032574	-16.425577
30	C	-11.224111	0.275685	-16.202036
31	C	-10.500682	0.034109	-14.824496
32	B	-14.802314	-2.162303	-14.551346
33	B	-12.145524	-1.684814	-15.183014
34	O	-11.390167	-0.980364	-14.185459
35	O	-16.155113	-2.615415	-14.503959
36	C	-10.429543	1.250791	-13.903310
37	H	-9.942002	0.973044	-12.962729
38	H	-9.843283	2.055242	-14.363828
39	H	-11.426078	1.630832	-13.670718

40	C	-9.120211	-0.624470	-14.965472
41	H	-8.381396	0.071533	-15.377987
42	H	-8.776108	-0.944203	-13.976650
43	H	-9.169857	-1.505892	-15.611748
44	C	-12.335090	1.333398	-16.132830
45	H	-11.925432	2.340637	-15.995774
46	H	-12.896113	1.312316	-17.072191
47	H	-13.033312	1.109552	-15.322206
48	C	-10.294884	0.539794	-17.385688
49	H	-10.889963	0.651938	-18.297509
50	H	-9.725792	1.465478	-17.235542
51	H	-9.593183	-0.282818	-17.539329
52	C	-17.438608	-1.183876	-15.988771
53	H	-17.943686	-2.072620	-16.380178
54	H	-18.117679	-0.330249	-16.092597
55	H	-16.544247	-1.015967	-16.593791
56	C	-18.309508	-1.780229	-13.697032
57	H	-18.986550	-0.919931	-13.630136
58	H	-18.849930	-2.599917	-14.181029
59	H	-18.046024	-2.098613	-12.686137
60	C	-16.162736	-0.278106	-12.371173
61	H	-15.353487	0.372300	-12.025720
62	H	-17.110262	0.110720	-11.981927
63	H	-15.997802	-1.277630	-11.957339
64	C	-16.370745	1.093724	-14.475457
65	H	-17.389410	1.444064	-14.269279
66	H	-15.669783	1.792670	-14.007942
67	H	-16.201851	1.113829	-15.553723
68	H	-13.842928	-3.061514	-16.200790
69	H	-11.795354	-3.881995	-15.097857
70	C	-13.273335	-4.877812	-16.162182
71	H	-12.964560	-5.790262	-15.696356
72	H	-14.266464	-4.990619	-16.544110
73	H	-12.606569	-4.644169	-16.965757

Cartesian coordinates of INT-3

S.No.	Atoms	Coordinates (Angstroms) X	Y	Z
1	C	-13.831763	-5.735345	-12.948223
2	C	-13.017301	-4.882945	-12.096864
3	N	-14.164436	-5.342670	-14.143750
4	C	-11.857193	-2.852553	-11.902006
5	C	-12.699030	-5.233432	-10.779179
6	C	-11.513641	-3.148385	-10.576774
7	C	-11.936098	-4.352836	-10.006756
8	N	-12.595845	-3.703255	-12.651405
9	H	-11.549815	-1.943279	-12.407175
10	H	-10.921676	-2.439977	-10.009520
11	H	-11.679589	-4.602054	-8.983331
12	H	-13.049638	-6.175373	-10.372165
13	C	-14.955859	-6.211374	-14.966652
14	C	-16.053139	-5.670296	-15.654425
15	C	-14.647120	-7.578195	-15.079285
16	C	-16.857401	-6.513959	-16.425847
17	H	-16.261340	-4.610637	-15.552573
18	C	-15.446810	-8.406211	-15.873298
19	H	-13.770035	-7.978984	-14.581118
20	C	-16.558411	-7.878970	-16.541060
21	H	-17.716982	-6.102167	-16.944686
22	H	-15.196750	-9.457336	-15.974397
23	H	-17.180286	-8.523252	-17.154089
24	H	-14.179483	-6.687093	-12.546259
25	Ir	-13.239966	-3.375964	-14.796810
26	O	-14.787851	-0.762084	-14.310824
27	C	-16.152342	-0.306142	-13.906078
28	C	-17.071112	-1.431048	-14.519613
29	O	-11.906373	-1.032574	-16.425577
30	C	-11.224111	0.275685	-16.202036
31	C	-10.500682	0.034109	-14.824496
32	B	-14.802314	-2.162303	-14.551346
33	B	-12.145524	-1.684814	-15.183014
34	O	-11.390167	-0.980364	-14.185459
35	O	-16.155113	-2.615415	-14.503959
36	C	-10.429543	1.250791	-13.903310
37	H	-9.942002	0.973044	-12.962729
38	H	-9.843283	2.055242	-14.363828
39	H	-11.426078	1.630832	-13.670718
40	C	-9.120211	-0.624470	-14.965472
41	H	-8.381396	0.071533	-15.377987
42	H	-8.776108	-0.944203	-13.976650
43	H	-9.169857	-1.505892	-15.611748
44	C	-12.335090	1.333398	-16.132830
45	H	-11.925432	2.340637	-15.995774
46	H	-12.896113	1.312316	-17.072191
47	H	-13.033312	1.109552	-15.322206
48	C	-10.294884	0.539794	-17.385688
49	H	-10.889963	0.651938	-18.297509
50	H	-9.725792	1.465478	-17.235542
51	H	-9.593183	-0.282818	-17.539329
52	C	-17.438608	-1.183876	-15.988771
53	H	-17.943686	-2.072620	-16.380178
54	H	-18.117679	-0.330249	-16.092597
55	H	-16.544247	-1.015967	-16.593791
56	C	-18.309508	-1.780229	-13.697032
57	H	-18.986550	-0.919931	-13.630136
58	H	-18.849930	-2.599917	-14.181029
59	H	-18.046024	-2.098613	-12.686137
60	C	-16.162736	-0.278106	-12.371173
61	H	-15.353487	0.372300	-12.025720
62	H	-17.110262	0.110720	-11.981927
63	H	-15.997802	-1.277630	-11.957339
64	C	-16.370745	1.093724	-14.475457
65	H	-17.389410	1.444064	-14.269279
66	H	-15.669783	1.792670	-14.007942
67	H	-16.201851	1.113829	-15.553723
68	H	-13.842928	-3.061514	-16.200790
69	C	-11.360118	-4.034453	-15.188557
70	H	-11.113469	-3.823310	-16.208107
71	H	-10.666316	-3.537142	-14.543406
72	H	-11.309715	-5.089993	-15.020644
73	H	-13.265609	-4.530094	-15.846061

Cartesian coordinates of TS-2

S.No.	Atoms	Coordinates (Angstroms) X	Y	Z
1	C	-13.831763	-5.735345	-12.948223
2	C	-13.017301	-4.882945	-12.096864
3	N	-14.164436	-5.342670	-14.143750
4	C	-11.857193	-2.852553	-11.902006
5	C	-12.699030	-5.233432	-10.779179
6	C	-11.513641	-3.148385	-10.576774
7	C	-11.936098	-4.352836	-10.006756
8	N	-12.595845	-3.703255	-12.651405
9	H	-11.549815	-1.943279	-12.407175
10	H	-10.921676	-2.439977	-10.009520
11	H	-11.679589	-4.602054	-8.983331
12	H	-13.049638	-6.175373	-10.372165
13	C	-14.955859	-6.211374	-14.966652
14	C	-16.053139	-5.670296	-15.654425
15	C	-14.647120	-7.578195	-15.079285
16	C	-16.857401	-6.513959	-16.425847
17	H	-16.261340	-4.610637	-15.552573
18	C	-15.446810	-8.406211	-15.873298
19	H	-13.770035	-7.978984	-14.581118
20	C	-16.558411	-7.878970	-16.541060
21	H	-17.716982	-6.102167	-16.944686
22	H	-15.196750	-9.457336	-15.974397
23	H	-17.180286	-8.523252	-17.154089
24	H	-14.179483	-6.687093	-12.546259
25	Ir	-13.239966	-3.375964	-14.796810
26	O	-14.787851	-0.762084	-14.310824
27	C	-16.152342	-0.306142	-13.906078
28	C	-17.071112	-1.431048	-14.519613
29	O	-11.906373	-1.032574	-16.425577
30	C	-11.224111	0.275685	-16.202036
31	C	-10.500682	0.034109	-14.824496

32	B	-14.802314	-2.162303	-14.551346
33	B	-12.145524	-1.684814	-15.183014
34	O	-11.390167	-0.980364	-14.185459
35	O	-16.155113	-2.615415	-14.503959
36	C	-10.429543	1.250791	-13.903310
37	H	-9.942002	0.973044	-12.962729
38	H	-9.843283	2.055242	-14.363828
39	H	-11.426078	1.630832	-13.670718
40	C	-9.120211	-0.624470	-14.965472
41	H	-8.381396	0.071533	-15.377987
42	H	-8.776108	-0.944203	-13.976650
43	H	-9.169857	-1.505892	-15.611748
44	C	-12.335090	1.333398	-16.132830
45	H	-11.925432	2.340637	-15.995774
46	H	-12.896113	1.312316	-17.072191
47	H	-13.033312	1.109552	-15.322206
48	C	-10.294884	0.539794	-17.385688
49	H	-10.889963	0.651938	-18.297509
50	H	-9.725792	1.465478	-17.235542
51	H	-9.593183	-0.282818	-17.539329
52	C	-17.438608	-1.183876	-15.988771
53	H	-17.943686	-2.072620	-16.380178
54	H	-18.117679	-0.330249	-16.092597
55	H	-16.544247	-1.015967	-16.593791
56	H	-18.309508	-1.780229	-13.697032
57	H	-18.986550	-0.919931	-13.630136
58	H	-18.849930	-2.599917	-14.181029
59	H	-18.046024	-2.098613	-12.686137
60	C	-16.162736	-0.278106	-12.371173
61	H	-15.353487	0.372300	-12.025720
62	H	-17.110262	0.110720	-11.981927
63	H	-15.997802	-1.277630	-11.957339
64	C	-16.370745	1.093724	-14.475457
65	H	-17.389410	1.444064	-14.269279
66	H	-15.669783	1.792670	-14.007942
67	H	-16.201851	1.113829	-15.553723
68	H	-13.842928	-3.061514	-16.200790
69	C	-11.360118	-4.034453	-15.188557
70	H	-11.113469	-3.823310	-16.208107
71	H	-10.666316	-3.537142	-14.543406
72	H	-11.309715	-5.089993	-15.020644
73	H	-13.265609	-4.530094	-15.846061

Cartesian coordinates of INT-4

S.No.	Atoms	Coordinates (Angstroms) X	Y	Z
1	C	-14.458348	-5.433514	-13.016727
2	C	-13.565883	-4.696650	-12.136223
3	N	-14.687958	-5.006695	-14.224723
4	C	-12.142864	-2.845781	-11.900412
5	C	-13.349257	-5.078849	-10.806776
6	C	-11.893903	-3.177315	-10.562545
7	C	-12.500893	-4.307451	-10.007166
8	N	-12.963909	-3.590790	-12.676136
9	H	-11.693238	-1.991523	-12.394917
10	H	-11.230947	-2.554101	-9.974213
11	H	-12.320228	-4.582815	-8.974286
12	H	-13.842510	-5.960130	-10.411955
13	C	-15.560961	-5.762706	-15.075884
14	C	-16.545672	-5.079221	-15.805962
15	C	-15.441275	-7.159905	-15.174446
16	C	-17.429835	-5.808297	-16.606211
17	H	-16.608178	-4.000238	-15.713838
18	C	-16.317888	-7.874278	-15.997121
19	H	-14.647818	-7.675190	-14.642477
20	C	-17.319448	-7.202367	-16.707727
21	H	-18.203661	-5.284692	-17.158185
22	H	-16.212802	-8.950619	-16.086905
23	H	-18.001361	-7.758241	-17.343046
24	H	-14.949918	-6.324942	-12.626826
25	Ir	-13.475065	-3.192012	-14.845115
26	O	-14.661605	-0.385181	-14.422833
27	C	-15.963691	0.258648	-14.071270
28	C	-17.006218	-0.731944	-14.717675
29	O	-10.698181	0.271425	-15.666623
30	C	-9.720792	-0.245052	-14.679494
31	C	-10.385044	-1.601807	-14.235295
32	B	-14.861581	-1.771444	-14.661491
33	B	-11.982141	-0.271840	-15.444952
34	O	-11.833248	-1.324342	-14.468585
35	O	-16.265061	-2.031924	-14.665124
36	C	-10.202464	-1.965703	-12.762813
37	H	-10.726921	-2.902630	-12.546842
38	H	-9.141448	-2.109051	-12.524875
39	H	-10.607664	-1.190602	-12.109634
40	C	-10.017853	-2.787849	-15.139605
41	H	-8.977945	-3.100161	-14.993012
42	H	-10.668076	-3.634514	-14.897175
43	H	-10.162542	-2.536710	-16.194609
44	C	-9.671206	0.806958	-13.562070
45	H	-8.952847	0.532692	-12.781127
46	H	-9.362938	1.763036	-13.996205
47	H	-10.659644	0.946099	-13.116689
48	C	-8.359269	-0.380845	-15.359246
49	H	-8.005003	0.608609	-15.665172
50	H	-7.620398	-0.808042	-14.670137
51	H	-8.413858	-1.010368	-16.249977
52	C	-17.280225	-0.446265	-16.200199
53	H	-17.888894	-1.258918	-16.609204
54	H	-17.829599	0.492673	-16.331271
55	H	-16.349077	-0.408386	-16.770859
56	C	-18.311207	-0.900046	-13.942472
57	H	-18.864071	0.046393	-13.902882
58	H	-18.941765	-1.640044	-14.445461
59	H	-18.132787	-1.244960	-12.921737
60	C	-16.027835	0.298444	-12.537930
61	H	-15.149583	0.832510	-12.162838
62	H	-16.926055	0.817787	-12.185809
63	H	-16.019189	-0.711421	-12.116495
64	C	-15.963724	1.671319	-14.650819
65	H	-16.930803	2.161168	-14.484291
66	H	-15.190470	2.269336	-14.157971
67	H	-15.753220	1.660331	-15.721872
68	H	-14.079809	-3.310725	-16.278221
69	H	-12.222099	-4.024223	-15.258759
70	C	-13.387356	0.206020	-16.165729
71	H	-13.778136	-0.598162	-16.753506
72	H	-14.099247	0.477377	-15.414413
73	H	-13.195944	1.048731	-16.796681

Cartesian coordinates of INT-5

S.No.	Atoms	Coordinates (Angstroms) X	Y	Z
1	C	-13.497862	-5.738790	-13.700062
2	c	-13.071552	-4.790677	-12.691467
3	N	-13.442749	-5.413773	-14.960612
4	C	-12.175296	-2.661794	-12.262139
5	C	-13.037370	-5.114050	-11.327317
6	C	-12.108432	-2.937915	-10.893759
7	C	-12.554144	-4.176149	-10.414673
8	N	-12.661418	-3.564760	-13.147279
9	H	-11.830114	-1.728579	-12.692699
10	H	-11.710830	-2.188918	-10.218926
11	H	-12.515491	-4.407389	-9.356140
12	H	-13.375784	-6.091202	-11.000841
13	C	-13.769162	-6.375170	-15.968529
14	C	-14.370898	-5.926884	-17.155588
15	C	-13.480543	-7.743663	-15.806458
16	C	-14.718981	-6.843474	-18.150172
17	H	-14.544693	-4.866045	-17.283624
18	C	-13.819504	-8.652002	-16.812978
19	H	-12.958233	-8.089098	-14.920739
20	C	-14.447729	-8.207955	-17.983133
21	H	-15.190373	-6.489818	-19.061059
22	H	-13.580771	-9.703270	-16.688071
23	H	-14.706721	-8.915279	-18.764115

24	H	-13.851108	-6.715916	-13.373399
25	Ir	-12.733932	-3.305017	-15.311165
26	O	-15.351845	-1.070858	-14.535231
27	C	-16.311206	-0.975284	-13.374861
28	C	-16.928156	-2.432694	-13.332297
29	O	-12.034610	-1.891473	-15.917082
30	C	-12.744304	-0.581167	-15.959185
31	C	-11.617403	0.391549	-16.480065
32	B	-15.048880	-2.410925	-14.754791
33	B	-10.631559	-1.695530	-15.818761
34	O	-10.374928	-0.294349	-16.013066
35	O	-15.844894	-3.258980	-13.982295
36	C	-11.639712	1.795753	-15.878080
37	H	-10.793935	2.374062	-16.264983
38	H	-12.562882	2.322314	-16.149124
39	H	-11.562347	1.764845	-14.789028
40	C	-11.525882	0.457116	-18.011452
41	H	-12.389270	0.973873	-18.445342
42	H	-10.621350	1.009178	-18.287558
43	H	-11.457218	-0.546168	-18.440731
44	C	-13.198197	-0.285327	-14.522162
45	H	-13.761163	0.653165	-14.461716
46	H	-13.846692	-1.100127	-14.185999
47	H	-12.344613	-0.239749	-13.840706
48	C	-13.950989	-0.729766	-16.885138
49	H	-14.647707	-1.458336	-16.458700
50	H	-14.479936	0.224999	-16.996286
51	H	-13.653926	-1.086511	-17.873263
52	C	-18.166806	-2.604581	-14.219383
53	H	-18.410666	-3.668721	-14.285636
54	H	-19.030761	-2.076928	-13.801964
55	H	-17.986884	-2.233090	-15.232409
56	C	-17.170919	-2.998997	-11.936405
57	H	-17.916047	-2.399681	-11.400690
58	H	-17.553068	-4.020856	-12.020091
59	H	-16.252388	-3.026506	-11.347161
60	C	-15.464824	-0.623509	-12.146958
61	H	-14.927367	0.308640	-12.342909
62	H	-16.093848	-0.480439	-11.261874
63	H	-14.726641	-1.399994	-11.931258
64	C	-17.301082	0.142781	-13.691988
65	H	-18.057629	0.224378	-12.902900
66	H	-16.765640	1.094831	-13.751169
67	H	-17.804028	-0.021439	-14.646527
68	H	-12.651674	-3.288862	-16.909697
69	C	-7.510157	-4.366276	-15.616292
70	C	-7.409756	-3.621168	-14.232885
71	B	-9.199940	-2.683146	-15.495037
72	C	-6.194118	-4.515343	-16.376020
73	H	-5.485228	-5.131706	-15.809876
74	H	-6.379277	-5.006432	-17.336945
75	H	-5.734084	-3.544944	-16.574149
76	C	-8.248460	-5.709508	-15.532082
77	H	-8.454985	-6.063620	-16.546899
78	H	-7.648303	-6.467744	-15.016786
79	H	-9.202839	-5.598345	-15.009096
80	C	-6.314086	-2.546201	-14.196380
81	H	-6.449390	-1.937444	-13.297637
82	H	-5.313270	-2.991654	-14.167797
83	H	-6.380682	-1.885416	-15.065773
84	C	-7.318114	-4.527392	-13.007029
85	H	-6.399737	-5.126601	-13.033508
86	H	-7.298884	-3.913823	-12.100967
87	H	-8.175289	-5.200438	-12.940905
88	O	-8.396574	-3.446097	-16.395660
89	O	-8.715372	-2.895548	-14.177686
90	H	-14.462252	-2.770441	-15.782506

Cartesian coordinates of TS-3

		Coordinates (Angstroms)		
S.No.	Atoms	X	Y	Z
1	C	-12.522559	-5.602415	-12.889516
2	c	-11.947830	-4.550219	-12.066522
3	N	-12.966147	-5.333184	-14.083204
4	C	-11.360636	-2.282873	-11.922785
5	c	-11.527280	-4.780300	-10.750988
6	C	-10.929979	-2.453444	-10.600959
7	C	-11.010954	-3.715918	-10.006238
8	N	-11.861047	-3.311607	-12.645417
9	H	-11.311848	-1.334212	-12.446345
10	H	-10.536499	-1.603917	-10.055506
11	H	-10.681397	-3.869983	-8.984984
12	H	-11.610740	-5.773654	-10.324231
13	C	-13.513899	-6.394520	-14.877998
14	C	-14.725897	-6.174015	-15.550502
15	C	-12.857831	-7.633750	-14.978438
16	C	-15.291800	-7.213629	-16.293907
17	H	-15.204244	-5.204808	-15.458742
18	H	-13.423811	-8.657484	-15.744733
19	H	-11.898234	-7.780369	-14.492890
20	C	-14.645654	-8.453726	-16.396752
21	H	-16.237745	-7.052171	-16.800627
22	H	-12.907326	-9.607430	-15.836708
23	H	-15.085614	-9.250113	-16.988222
24	H	-12.600732	-6.604561	-12.467734
25	Ir	-12.603117	-3.204874	-14.781468
26	O	-14.776914	-1.081981	-14.299362
27	C	-16.206617	-0.993820	-13.873077
28	C	-16.806329	-2.331944	-14.452511
29	O	-12.046211	-0.380427	-16.015661
30	C	-12.004813	1.097433	-15.912329
31	C	-11.090214	1.315044	-14.649207
32	B	-14.425848	-2.440831	-14.520613
33	B	-11.777256	-0.986335	-14.769320
34	O	-11.326001	0.057318	-13.880288
35	O	-15.610536	-3.233019	-14.439545
36	C	-11.477305	2.495142	-13.759551
37	H	-10.806396	2.540743	-12.895068
38	H	-11.389358	3.441663	-14.306617
39	H	-12.500162	2.395490	-13.391524
40	C	-9.590282	1.349349	-14.978339
41	H	-9.312390	2.272742	-15.498490
42	H	-9.020180	1.295933	-14.045314
43	H	-9.305633	0.496856	-15.602256
44	C	-13.460859	1.534645	-15.696470
45	H	-13.549086	2.624964	-15.628969
46	H	-14.058275	1.190573	-16.546351
47	H	-13.872622	1.078145	-14.792704
48	C	-11.453961	1.667200	-17.218536
49	H	-12.139446	1.427836	-18.037639
50	H	-11.362852	2.758788	-17.159922
51	H	-10.476339	1.245791	-17.462155
52	C	-17.249581	-2.217259	-15.917074
53	H	-17.508912	-3.214635	-16.286070
54	H	-18.131134	-1.574481	-16.018550
55	H	-16.440920	-1.831069	-16.542413
56	C	-17.895564	-2.979519	-13.600215
57	H	-18.774166	-2.326633	-13.531152
58	H	-18.208669	-3.921290	-14.061984
59	H	-17.541258	-3.198694	-12.590695
60	C	-16.199298	-0.941281	-12.338797
61	H	-15.584534	-0.094601	-12.018726
62	H	-17.209389	-0.808416	-11.935601
63	H	-15.770219	-1.854385	-11.914954
64	C	-16.795246	0.288513	-14.456732
65	H	-17.866763	0.362167	-14.234580
66	H	-16.295749	1.155762	-14.013083
67	H	-16.655010	0.332519	-15.538390
68	H	-13.187458	-3.590669	-16.175494
69	C	-8.645615	-5.784252	-15.788109
70	C	-8.177031	-4.358481	-16.041135
71	B	-10.377861	-4.253944	-14.941702
72	C	-8.661629	-6.590074	-17.100357
73	H	-7.658640	-6.727365	-17.446859
74	H	-9.112982	-7.544647	-16.927236
75	H	-9.224393	-6.058098	-17.838733
76	C	-7.679467	-6.502390	-14.827674
77	H	-7.986497	-7.520397	-14.708111

78	H	-6.688766	-6.473658	-15.230891
79	H	-7.691856	-6.012081	-13.876704
80	C	-7.976456	-4.119370	-17.549179
81	H	-7.882224	-3.069752	-17.734446
82	H	-7.088671	-4.620127	-17.874723
83	H	-8.819112	-4.502094	-18.086164
84	C	-6.819720	-4.107475	-15.358272
85	H	-6.099057	-4.805756	-15.729685
86	H	-6.492798	-3.110895	-15.570052
87	H	-6.924239	-4.231373	-14.300621
88	O	-10.040583	-5.718154	-15.183332
89	O	-9.234811	-3.412279	-15.491232
90	H	-14.142626	-3.469191	-14.919255

Cartesian coordinates of INT-6

		Coordinates (Angstroms)		
S.No.	Atoms	X	Y	Z
1	C	-12.522559	-5.602415	-12.889516
2	c	-11.947830	-4.550219	-12.066522
3	N	-12.966147	-5.333184	-14.083204
4	C	-11.360636	-2.282873	-11.922785
5	c	-11.527280	-4.780300	-10.750988
6	C	-10.929979	-2.453444	-10.600959
7	C	-11.010954	-3.715918	-10.006238
8	N	-11.861047	-3.311607	-12.645417
9	H	-11.311848	-1.334212	-12.446345
10	H	-10.536499	-1.603917	-10.055506
11	H	-10.681397	-3.869983	-8.984984
12	H	-11.610740	-5.773654	-10.324231
13	C	-13.513899	-6.394520	-14.877998
14	C	-14.725897	-6.174015	-15.550502
15	C	-12.857831	-7.633750	-14.978438
16	C	-15.291800	-7.213629	-16.293907
17	H	-15.204244	-5.204808	-15.458742
18	H	-13.423811	-8.657484	-15.744733
19	H	-11.898234	-7.780369	-14.492890
20	C	-14.645654	-8.453726	-16.396752
21	H	-16.237745	-7.052171	-16.800627
22	H	-12.907326	-9.607430	-15.836708
23	H	-15.085614	-9.250113	-16.988222
24	H	-12.600732	-6.604561	-12.467734
25	Ir	-12.603117	-3.204874	-14.781468
26	O	-14.776914	-1.081981	-14.299362
27	C	-16.206617	-0.993820	-13.873077
28	C	-16.806329	-2.331944	-14.452511
29	O	-12.046211	-0.380427	-16.015661
30	C	-12.004813	1.097433	-15.912329
31	C	-11.090214	1.315044	-14.649207
32	B	-14.425848	-2.440831	-14.520613
33	B	-11.777256	-0.986335	-14.769320
34	O	-11.326001	0.057318	-13.880288
35	O	-15.610536	-3.233019	-14.439545
36	C	-11.477305	2.495142	-13.759551
37	H	-10.806396	2.540743	-12.895068
38	H	-11.389358	3.441663	-14.306617
39	H	-12.500162	2.395490	-13.391524
40	C	-9.590282	1.349349	-14.978339
41	H	-9.312390	2.272742	-15.498490
42	H	-9.020180	1.295933	-14.045314
43	H	-9.305633	0.496856	-15.602256
44	C	-13.460859	1.534645	-15.696470
45	H	-13.549086	2.624964	-15.628969
46	H	-14.058275	1.190573	-16.546351
47	H	-13.872622	1.078145	-14.792704
48	C	-11.453961	1.667200	-17.218536
49	H	-12.139446	1.427836	-18.037639
50	H	-11.362852	2.758788	-17.159922
51	H	-10.476339	1.245791	-17.462155
52	C	-17.249581	-2.217259	-15.917074
53	H	-17.508912	-3.214635	-16.286070
54	H	-18.131134	-1.574481	-16.018550
55	H	-16.440920	-1.831069	-16.542413
56	C	-17.895564	-2.979519	-13.600215
57	H	-18.774166	-2.326633	-13.531152
58	H	-18.208669	-3.921290	-14.061984
59	H	-17.541258	-3.198694	-12.590695
60	C	-16.199298	-0.941281	-12.338797
61	H	-15.584534	-0.094601	-12.018726
62	H	-17.209389	-0.808416	-11.935601
63	H	-15.770219	-1.854385	-11.914954
64	C	-16.795246	0.288513	-14.456732
65	H	-17.866763	0.362167	-14.234580
66	H	-16.295749	1.155762	-14.013083
67	H	-16.655010	0.332519	-15.538390
68	H	-13.187458	-3.590669	-16.175494
69	C	-8.645615	-5.784252	-15.788109
70	C	-8.177031	-4.358481	-16.041135
71	B	-10.377861	-4.253944	-14.941702
72	C	-8.661629	-6.590074	-17.100357
73	H	-7.658640	-6.727365	-17.446859
74	H	-9.112982	-7.544647	-16.927236
75	H	-9.224393	-6.058098	-17.838733
76	C	-7.679467	-6.502390	-14.827674
77	H	-7.986497	-7.520397	-14.708111
78	H	-6.688766	-6.473658	-15.230891
79	H	-7.691856	-6.012081	-13.876704
80	C	-7.976456	-4.119370	-17.549179
81	H	-7.882224	-3.069752	-17.734446
82	H	-7.088671	-4.620127	-17.874723
83	H	-8.819112	-4.502094	-18.086164
84	C	-6.819720	-4.107475	-15.358272
85	H	-6.099057	-4.805756	-15.729685
86	H	-6.492798	-3.110895	-15.570052
87	H	-6.924239	-4.231373	-14.300621
88	O	-10.040583	-5.718154	-15.183332
89	O	-9.234811	-3.412279	-15.491232
90	H	-14.142626	-3.469191	-14.919255

Cartesian coordinates of TS-4

		Coordinates (Angstroms)		
S.No.	Atoms	X	Y	Z
1	C	-12.522559	-5.602415	-12.889516
2	C	-11.947830	-4.550219	-12.066522
3	N	-12.966147	-5.333184	-14.083204
4	C	-11.360636	-2.282873	-11.922785
5	C	-11.527280	-4.780300	-10.750988
6	C	-10.929979	-2.453444	-10.600959
7	C	-11.010954	-3.715918	-10.006238
8	N	-11.861047	-3.311607	-12.645417
9	H	-11.311848	-1.334212	-12.446345
10	H	-10.536499	-1.603917	-10.055506
11	H	-10.681397	-3.869983	-8.984984
12	H	-11.610740	-5.773654	-10.324231
13	C	-13.513899	-6.394520	-14.877998
14	C	-14.725897	-6.174015	-15.550502
15	C	-12.857831	-7.633750	-14.978438
16	C	-15.291800	-7.213629	-16.293907
17	H	-15.204244	-5.204808	-15.458742
18	C	-13.423811	-8.657484	-15.744733
19	H	-11.898234	-7.780369	-14.492890
20	C	-14.645654	-8.453726	-16.396752
21	H	-16.237745	-7.052171	-16.800627
22	H	-12.907326	-9.607430	-15.836708
23	H	-15.085614	-9.250113	-16.988222
24	H	-12.600732	-6.604561	-12.467734
25	Ir	-12.603117	-3.204874	-14.781468
26	O	-14.776914	-1.081981	-14.299362
27	C	-16.206617	-0.993820	-13.873077
28	C	-16.806329	-2.331944	-14.452511
29	O	-12.046211	-0.380427	-16.015661
30	C	-12.004813	1.097433	-15.912329
31	C	-11.090214	1.315044	-14.649207
32	B	-14.425848	-2.440831	-14.520613
33	B	-11.777256	-0.986335	-14.769320
34	O	-11.326001	0.057318	-13.880288
35	O	-15.610536	-3.233019	-14.439545

36	C	-11.477305	2.495142	-13.759551	64	C	-16.795246	0.288513	-14.456732
37	H	-10.806396	2.540743	-12.895068	65	H	-17.866763	0.362167	-14.234580
38	H	-11.389358	3.441663	-14.306617	66	H	-16.295749	1.155762	-14.013083
39	H	-12.500162	2.395490	-13.391524	67	H	-16.655010	0.332519	-15.538390
40	C	-9.590282	1.349349	-14.978339	68	H	-13.187458	-3.590669	-16.175494
41	H	-9.312390	2.272742	-15.498490	69	C	-8.645615	-5.784252	-15.788109
42	H	-9.020180	1.295933	-14.045314	70	C	-8.177031	-4.358481	-16.041135
43	H	-9.305633	0.496856	-15.602256	71	B	-10.377861	-4.253944	-14.941702
44	C	-13.460859	1.534645	-15.696470	72	C	-8.661629	-6.590074	-17.100357
45	H	-13.549086	2.624964	-15.628969	73	H	-7.658640	-6.727365	-17.446859
46	H	-14.058275	1.190573	-16.546351	74	H	-9.112982	-7.544647	-16.927236
47	H	-13.872622	1.078145	-14.792704	75	H	-9.224393	-6.058098	-17.838733
48	C	-11.453961	1.667200	-17.218536	76	C	-7.679467	-6.502390	-14.827674
49	H	-12.139446	1.427836	-18.037639	77	H	-7.986497	-7.520397	-14.708111
50	H	-11.362852	2.758788	-17.159922	78	H	-6.688766	-6.473658	-15.230891
51	H	-10.476339	1.245791	-17.462155	79	H	-7.691856	-6.012081	-13.876704
52	C	-17.249581	-2.217259	-15.917074	80	C	-7.976456	-4.119370	-17.549179
53	H	-17.508912	-3.214635	-16.286070	81	H	-7.882224	-3.069752	-17.734446
54	H	-18.131134	-1.574481	-16.018550	82	H	-7.088671	-4.620127	-17.874723
55	H	-16.440920	-1.831069	-16.542413	83	H	-8.819112	-4.502094	-18.086164
56	C	-17.895564	-2.979519	-13.600215	84	C	-6.819720	-4.107475	-15.358272
57	H	-18.774166	-2.326633	-13.531152	85	H	-6.099057	-4.805756	-15.729685
58	H	-18.208669	-3.921290	-14.061984	86	H	-6.492798	-3.110895	-15.570052
59	H	-17.541258	-3.198694	-12.590695	87	H	-6.924239	-4.231373	-14.300621
60	C	-16.199298	-0.941281	-12.338797	88	C	-10.040583	-5.718154	-15.183332
61	H	-15.584534	-0.094601	-12.018726	89	O	-9.234811	-3.412279	-15.491232
62	H	-17.209389	-0.808416	-11.935601	90	H	-14.142626	-3.469191	-14.919255
63	H	-15.770219	-1.854385	-11.914954					

6.2. Ir^{I}-Ir^{III}-Ir^{I} catalytic cycle of pyrim-UiO-IrH catalyzed monoborylation of methane.

In pyrim-UiO-IrH catalyzed monoborylation of methane, a Ir^{I}-Ir^{III}-Ir^{I} catalytic cycle (Figure S17, SI) could be an alternative pathway compared to the Ir^{III}-Ir^{V}-Ir^{III} catalytic cycle as described in Figure 4 in the main manuscript. According to this cycle, Ir^{III}(diboryl)hydride (INT-A) undergoes reductive elimination of a B–H bond, resulting in the formation of the Ir^{I} boryl intermediate (INT-B), instead of oxidative addition to form a 7 coordinate, 18-electron Ir^{V} intermediate (INT-2, Figure 4, manuscript). Subsequent oxidative addition of methane yields Ir^{III}(boryl)(methyl)hydride (INT-C), and further reductive elimination of MeBpin and oxidative addition of B_2pin_2 regenerates INT-A. Alternatively, pyrim-Ir^{I}(Bpin) (INT B) reacts with CH_4 to form pyrim-Ir^{III}(Bpin)(CH_3)(H) (INT-C), which could undergo reductive elimination to give pyrim-Ir^{I}-CH_3 species. Then, pyrim-Ir^{I}-CH_3 reacts with B_2Pin_2 to give pyrim-Ir^{III}(CH_3)(Bpin)$_2$, which then gives CH_3Bpin and regenerates INT-B. However, these above two pathways via Ir^{I}-Ir^{III}-Ir^{I} catalytic cycle are unlikely due to the high barrier associated with the transformation of INT-B to INT-C, involving CH_4 C–H activation. DFT calculations reveal that the activation energy for methane mono borylation via Ir^{I}-Ir^{III}-Ir^{I} cycle is significantly higher compared to that of Ir^{III}-Ir^{V}-Ir^{III} catalytic cycle, as depicted in Figure 4 of the manuscript. Therefore, based on the DFT calculation, we propose that pyrim-UiO-IrH catalyzed methane borylation reaction likely occurs via Ir^{III}-Ir^{V}-Ir^{III} catalytic cycle.

a)

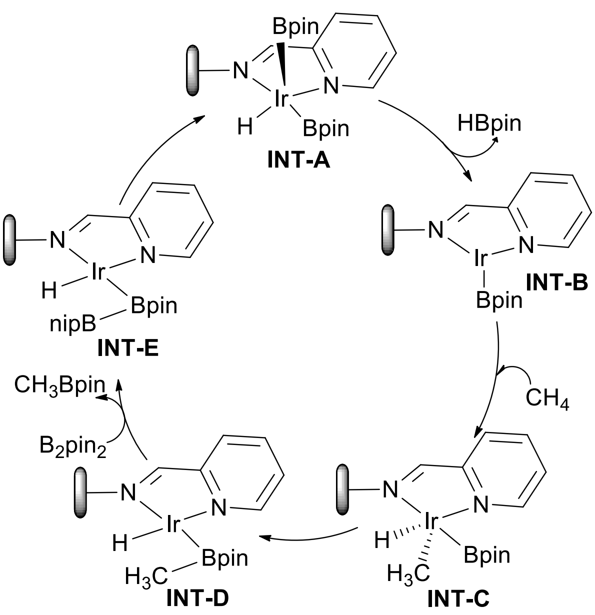

b)

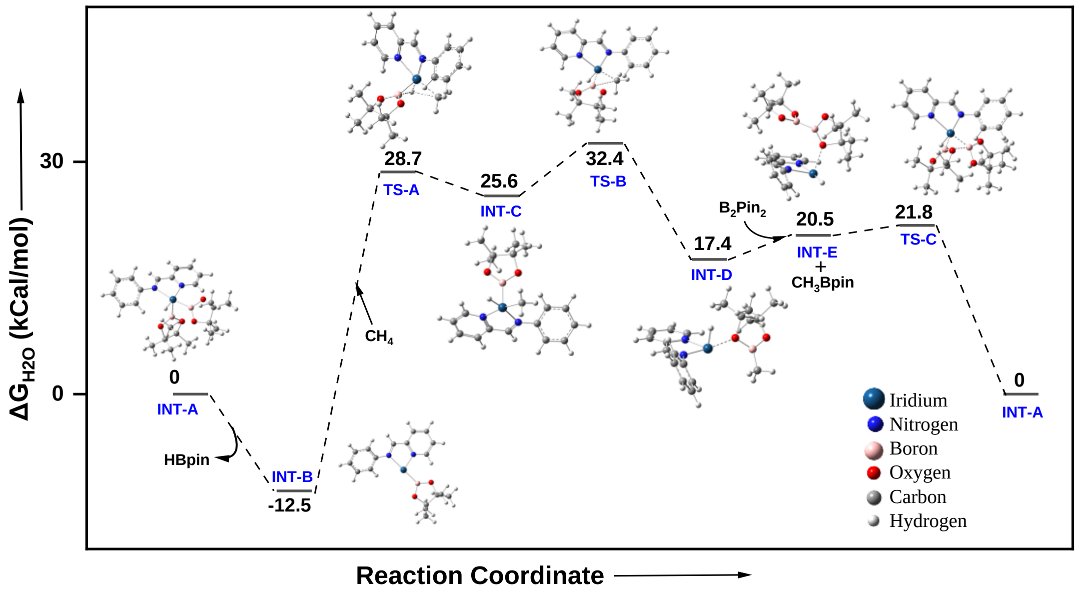

Figure S17. (a) Ir^{I}-Ir^{III}-Ir^{I} catalytic cycle of pyrim-UiO-IrH catalyzed monoborylation of methane. (b) DFT-calculated free energy profile at 403 K for Ir^{I}-Ir^{III}-Ir^{I} catalytic cycle of pyrim-UiO-IrH catalyzed methane borylation reaction. We used the Polarizable Continuum Model (PCM) using the integral equation formalism variant (IEFPCM) as the default SCRF method by using cyclohexane as the solvent for all the molecules in this DFT calculation at 403 K.

7. XAS analysis.

7.1. X-ray absorption spectroscopic analysis. X-ray Near-Edge Structure (XANES) and Extended X-ray Absorption Fine Structure (EXAFS) measurements have been carried out at the Energy-Scanning EXAFS beamLine (BL-9) at the Indus-2 Synchrotron Source at Raja Ramanna Centre for Advanced Technology (RRCAT), Indore, India.[14] All the measurements were performed at room temperature. This beamLine operates in the energy range of 4 keV to 25 keV. The beamLine optics consist of a Rh/Pt coated collimating meridional cylindrical mirror and the collimated beam reflected by the mirror is monochromatized by a Si (111) based double crystal monochromator (DCM). The second crystal of the DCM is a sagittal cylindrical crystal which is used for horizontal focusing of the beam while another Rh/Pt coated bendable post mirror facing downward is used for vertical focusing of the beam at the sample position. Two ionization chambers (300 mm length each) have been used for data collection in the transmission mode; one ionization chamber for measuring incident flux, the second one for measuring transmitted flux. For energy calibration, standard metal foils were used. Appropriate gas pressure and gas mixture have been chosen to achieve 10-20% absorption in the first ionization chamber and 70-90% absorption in the second ionization chamber to obtain a better signal-to-noise ratio. Pellets were made from powder samples for recording absorption spectra. Sample powder was mixed homogeneously with cellulose powder in appropriate proportion and pressed (2 Ton) into a 15 mm diameter disc. The amount of the sample was estimated such that to get a reasonable edge jump at a particular absorption edge of the element to be probed. Spectra were collected at the iridium L_3-edge in transmission mode and were calibrated against the reference spectrum of metallic iridium (11215 eV). Data were processed using Demeter software.[15] Metallic iridium pellet standard was used as a reference for energy calibration and was measured simultaneously with experimental samples.

7.2. XANES analysis. The oxidation states of the Ir species within pyrim-UiO-$IrCl_3$(THF) and pyrim-UiO-IrH were determined by the comparison of the energy of its L_3-edge positions to that of Ir(0) and IrO_2. The positions of the L_3-edge of pyrim-UiO-$IrCl_3$(THF) (11219.5 eV) was ~1.5 eV lower than IrO_2 (11221.0 eV), while L_3-edge of pyrim-UiO-IrH (11216.5 eV) was ~1.5 eV higher in energy to Ir(0) (11215 eV). We, therefore, conclude that Ir ion in pyrim-UiO-$IrCl_3$(THF) has +3 oxidation state and in pyrim-UiO-IrH has +1 oxidation state.

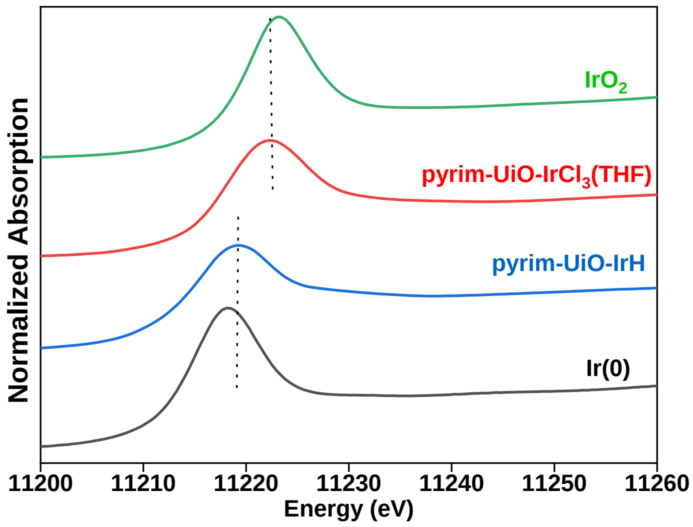

Figure S18. Ir L_3-edge XANES spectra of Ir(0) (black), pyrim-UiO-IrH (blue), pyrim-UiO-$IrCl_3$(THF) (red) and IrO_2(green).

7.3. EXAFS fitting using DFT optimized structures. The spectra were calibrated against the reference spectra and aligned to the first peak in the smoothed first derivative of the absorption spectrum, the background noise was removed, and the spectra were processed to obtain a normalized unit edge step. The fitting parameters of pyrim-UiO-$IrCl_3$ and pyrim-UiO-IrH are summarized in Table S4, and Table S5, respectively.

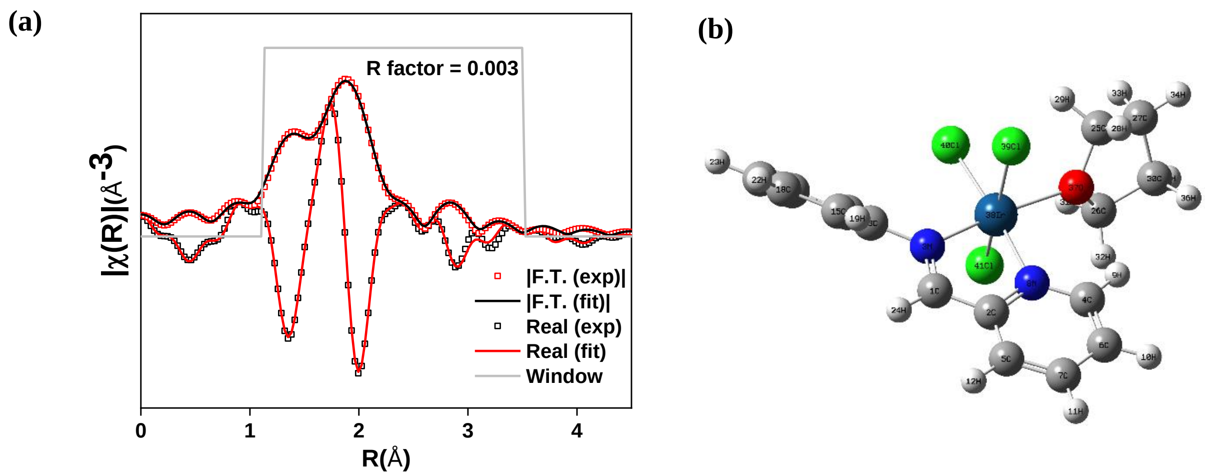

Figure S19. (a) EXAFS spectra (red and black hollow squares) and fits (red and black solid lines) of pyrim-UiO-$IrCl_3$ in the R space from 1.15 - 3.5 Å. (b) DFT optimised structure of (pyrim)$IrCl_3$(THF) molecule.

Table S4. Summary of the EXAFS fitting parameters of pyrim-UiO-IrCl$_3$.

Sample	**Pyrim-IrCl$_3$(THF)**	**Fitting range**	***k* 3-11 Å^{-1}** **R 1.15-3.5 Å**
Independent points	11	**R-factor**	0.003
Variables	10	**S_o^2**	0.55
Reduced chi-square	621	**ΔE_0(eV)**	6.18
R(Ir-H26) (Å)	1.56±0.06	**σ^2(Ir-H3) (Å^2)**	0.005±0.001
R(Ir-N3) (Å)	1.99±0.07	**σ^2(Ir-N3) (Å^2)**	0.003±0.004
R(Ir-N8) (Å)	1.99±0.07	**σ^2 (Ir-N8) (Å^2)**	0.003±0.004
R(Ir-Cl39) (Å)	2.37±0.08	**σ^2 (Ir-Cl39) (Å^2)**	0.006±0.006
R(Ir-Cl40) (Å)	2.37±0.08	**σ^2 (Ir-Cl40) (Å^2)**	0.006±0.006
R(Ir-Cl41) (Å)	2.37±0.08	**σ^2 (Ir-Cl41) (Å^2)**	0.006±0.004
R(Ir-C1) (Å)	2.80±0.04	**σ^2 (Ir-C1) (Å^2)**	0.002±0.004
R(Ir-C2) (Å)	2.80±0.04	**σ^2 (Ir-C2) (Å^2)**	0.002±0.001
R(Ir-C13) (Å)	3.02±0.05	**σ^2 (Ir-C13) (Å^2)**	0.002±0.001
R(Ir-C4) (Å)	3.02±0.05	**σ^2 (Ir-C4) (Å^2)**	0.002±0.001

(a)

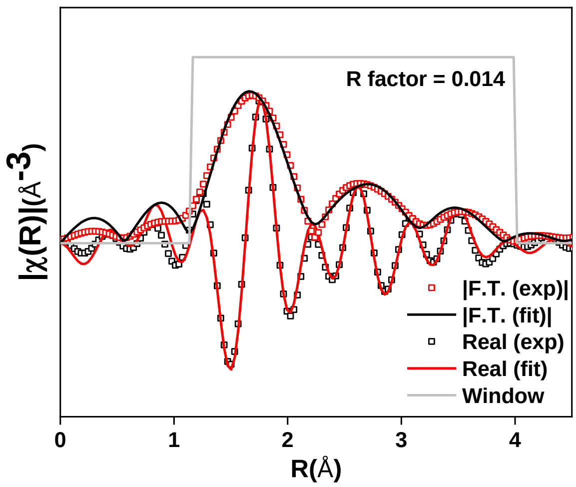

(b)

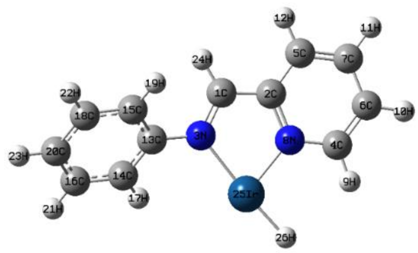

Figure S20. (a) EXAFS spectra (red and black hollow squares) and fits (red and black solid lines) of pyrim-UiO-IrH in the R space from 1.15 - 4.0 Å. (b) DFT optimised structure of pyrim-IrH.

Table S5. Summary of the EXAFS fitting parameters of pyrim-IrH.

Sample	Pyrim-IrH	Fitting range	***k*** **3-10.5 Å^{-1}** **R 1.15-4.0 Å**
Independent points	13	**R-factor**	0.017
Variables	11	**S_0^2**	0.81
Reduced chi-square	889	**ΔE_0(eV)**	9.65
R(Ir-N3) (Å)	1.99±0.06	**σ^2(Ir-N3) (Å^2)**	0.008±0.004
R(Ir-N8) (Å)	1.99±0.06	**σ^2 (Ir-N8) (Å^2)**	0.008±0.004
R(Ir-C1) (Å)	2.70±0.08	**σ^2 (Ir-C1) (Å^2)**	0.009±0.006
R(Ir-C2) (Å)	2.70±0.08	**σ^2 (Ir-C2) (Å^2)**	0.009±0.006
R(Ir-C13) (Å)	3.01±0.07	**σ^2 (Ir-C13) (Å^2)**	0.009±0.004
R(Ir-C4) (Å)	3.01±0.07	**σ^2 (Ir-C4) (Å^2)**	0.009±0.004
R(Ir-C14) (Å)	3.26±0.09	**σ^2 (Ir-C14) (Å^2)**	0.003±0.001
R(Ir-C15) (Å)	4.31±0.05	**σ^2 (Ir-C15) (Å^2)**	0.005±0.001
R(Ir-C5) (Å)	4.31±0.05	**σ^2 (Ir-C5) (Å^2)**	0.005±0.001
R(Ir-C4) (Å)	4.32±0.05	**σ^2 (Ir-C4) (Å^2)**	0.005±0.001

8. XPS analysis. All the binding energies were corrected with reference to the C1s peak at 284.8 eV. MULTIPAK software was used for peak analysis and de-convolution studies.

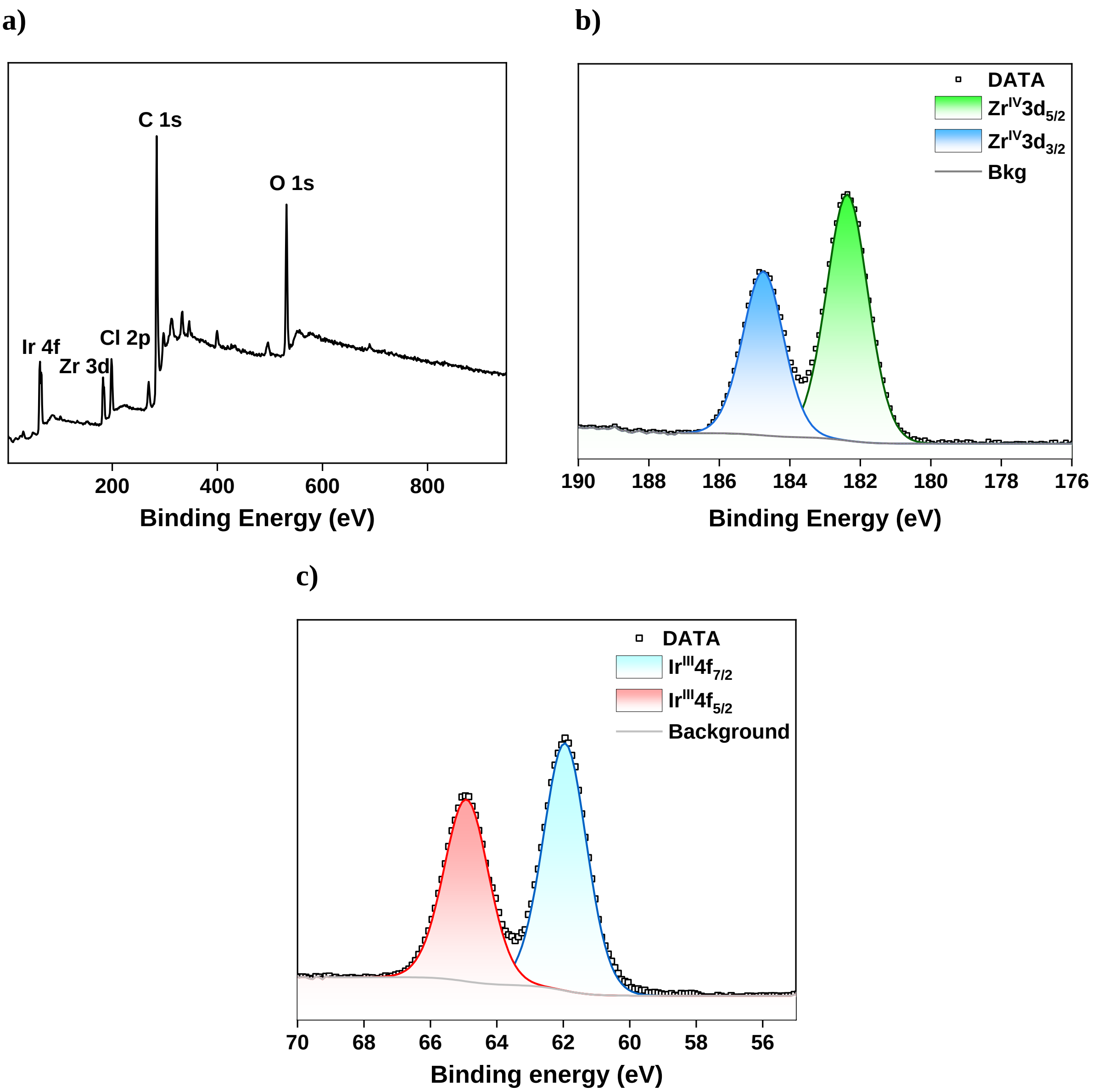

Figure S21. a) Raw XPS data of pyrim-UiO-$IrCl_3$; b) Zr 3d XPS spectrum of pyrim-UiO-$IrCl_3$; c) Ir 4f XPS spectrum of pyrim-UiO-$IrCl_3$.

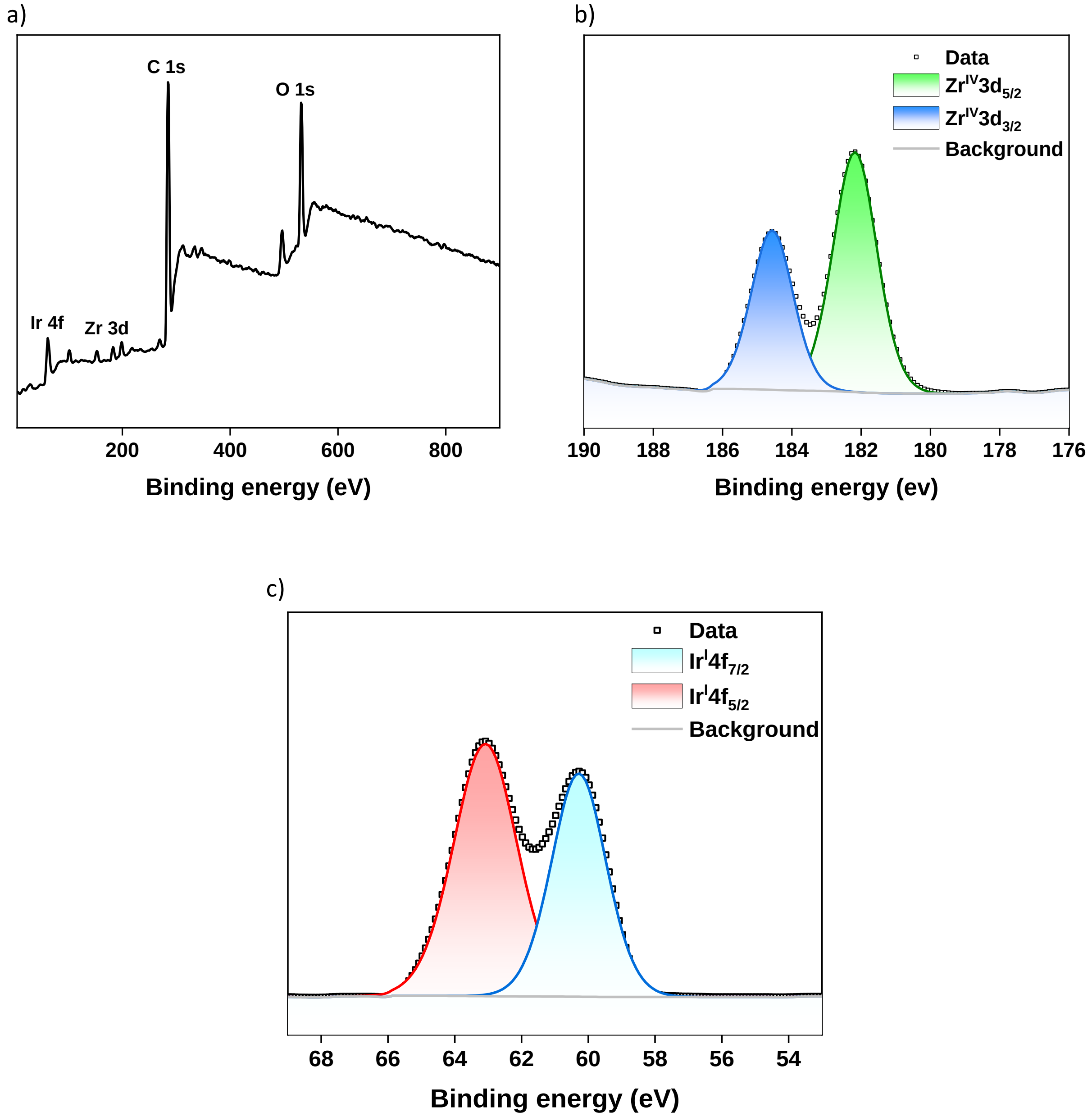

Figure S22. a) Raw XPS data of pyrim-UiO-IrH; b) Zr 3d XPS spectrum of pyrim-UiO-IrH; c) Ir 4f XPS spectrum of pyrim-UiO-IrH.

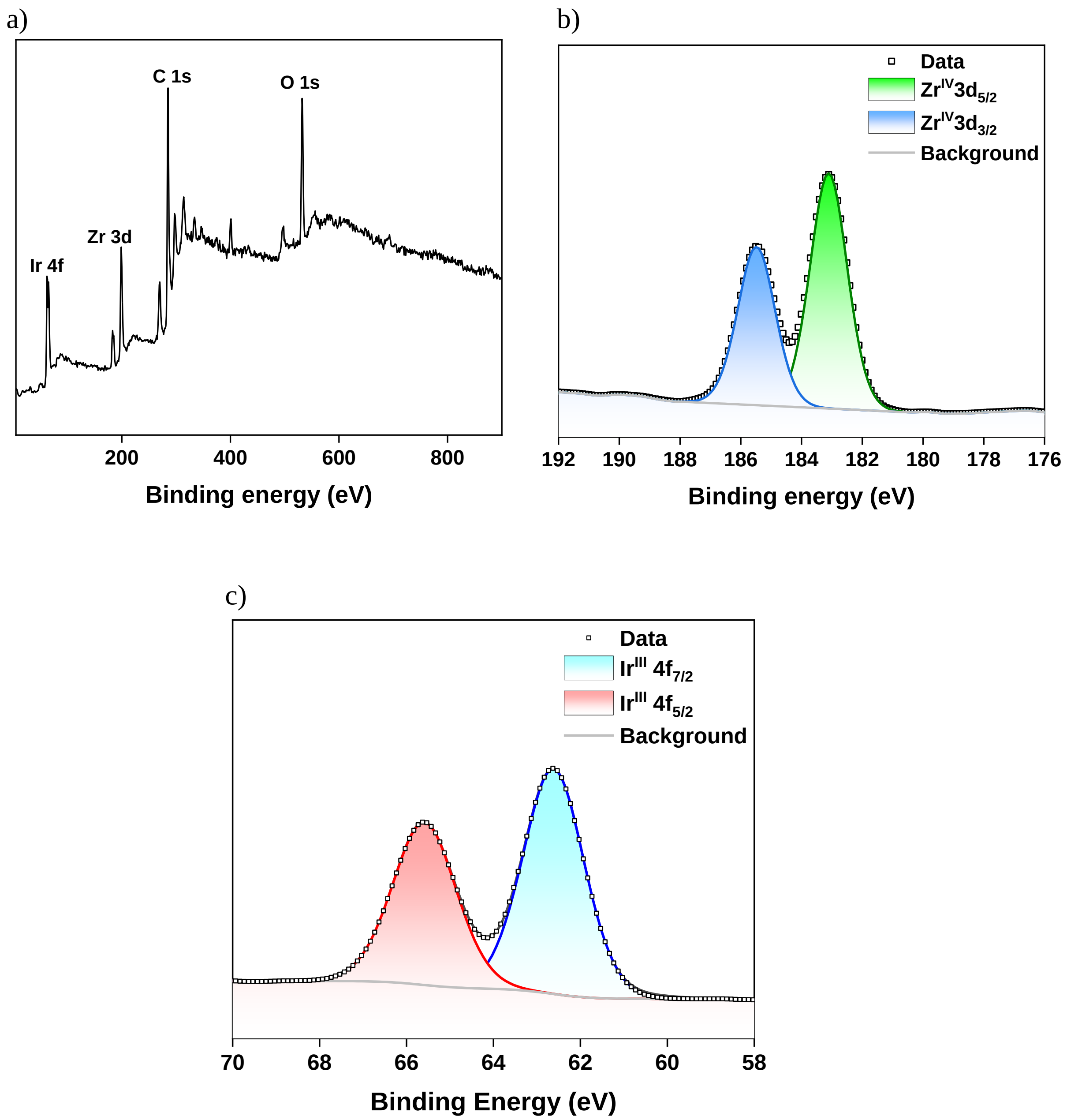

Figure S23. a) Raw XPS data of pyrim-UiO-IrH(Bpin)$_2$; b) Zr 3d XPS spectrum of pyrim-UiO-IrH(Bpin)$_2$; c) Ir 4f XPS spectrum of pyrim-UiO-IrH(Bpin)$_2$.

Table S6. Comparison of catalytic activity of pyrim-UiO-IrH with that of other reported catalysts in borylation of CH_4.

Catalysts	CH_4 pressure	Temperature/ Reaction time	Yield (TON) of CH_3Bpin	Reference
[Ir(COD)Cl]$_2$ + 2 equiv. dmpe	34.47 bar	150 °C (16 h)	52 % (104)	*Science* **2016**, *351* (6280), 1424-1427.
(MesH)Ir(Bpin)$_3$ + 3,4,7,8-tetramethylphenanthroline	35 bar	150 °C (14 h)	45 % (15)	*Science* **2016**, *351* (6280), 1421-1424.
(dmpe)Ir(COD)Cl	500 psi	150 °C (16 h)	31% (153)	*ACS Catal.* **2018**, *8* (11), 10021-10031.
UiO-67-Mix-Ir (0.49)	34 bar	150 °C (14 h)	19.5% (67)	*Nat. Catal.* **2018**, *1* (5), 356-362.
Zr-P1-Ir (0.3)	50 bar	110 °C (15 h)	38.0% (127)	*J. Am. Chem. Soc.* **2019**, *141*, 11196−11203.
CAL-3-Ir	34 bar	150 °C (9 h)	29% (126)	*Angew. Chem. Int. Ed.* **2019**, *58*, 10671 – 10676.
[(dmpe)Ir(cod)]-SiO$_2$ (0.069)	34.47 bar	150 °C (16 h)	82.8% (1204)	*J. Am. Chem. Soc.* **2023**, *145*, 7992−8000.
Pyrim-UiO-IrH (0.5)	**40 bar**	**130 °C (24 h)**	**98% (196)**	**This work**

9. References.

1 J. H. Cavka, S. Jakobsen, U. Olsbye, N. Guillou, C. Lamberti, S. Bordiga and K. P. Lillerud, *J. Am. Chem. Soc.*, 2008, **130**, 13850–13851.
2 K. Manna, T. Zhang, M. Carboni, C. W. Abney and W. Lin, *J. Am. Chem. Soc.*, 2014, **136**, 13182–13185.
3 T. Zhang, K. Manna and W. Lin, *J. Am. Chem. Soc.*, 2016, **138**, 3241–3249.
4 R. Newar, W. Begum, N. Antil, S. Shukla, A. Kumar, N. Akhtar, Balendra and K. Manna, *Inorg. Chem.*, 2020, **59**, 10473–10481.
5 R. Newar, N. Akhtar, N. Antil, A. Kumar, S. Shukla, W. Begum and K. Manna, *Angew. Chem. Int. Ed.*, 2021, **60**, 10964–10970.
6 X. Zhang, Z. Huang, M. Ferrandon, D. Yang, L. Robison, P. Li, T. C. Wang, M. Delferro and O. K. Farha, *Nat. Catal.*, 2018, **1**, 356–362.
7 X. Feng, Y. Song, Z. Li, M. Kaufmann, Y. Pi, J. S. Chen, Z. Xu, Z. Li, C. Wang and W. Lin, *J. Am. Chem. Soc.*, 2019, **141**, 11196–11203.
8 S. N. Tambat, P. K. Sane, S. Suresh, N. Varadan O., A. B. Pandit and S. M. Sontakke, *Adv. Powder Technol.*, 2018, **29**, 2626–2632.
9 H. Park, E. N. Brothers and K. M. Merz, *J. Am. Chem. Soc.*, 2005, **127**, 4232–4241.
10 T. Vreven, K. S. Byun, I. Komáromi, S. Dapprich, J. A. Montgomery, K. Morokuma and M. J. Frisch, *J. Chem. Theory Comput.*, 2006, **2**, 815–826.

11 M. Araújo, B. Lasorne, A. L. Magalhães, G. A. Worth, M. J. Bearpark and M. A. Robb, *J. Chem. Phys.*, 2009, **131**, 144301.
12 V. Yempally, S. J. Kyran, R. K. Raju, W. Y. Fan, E. N. Brothers, D. J. Darensbourg and A. A. Bengali, *Inorg. Chem.*, 2014, **53**, 4081–4088.
13 S. Canneaux, F. Bohr and E. Henon, *J. Comput. Chem.*, 2014, **35**, 82–93.
14 A. K. Poswal, A. Agrawal, A. K. Yadav, C. Nayak, S. Basu, S. R. Kane, C. K. Garg, D. Bhattachryya, S. N. Jha and N. K. Sahoo, Thapar University, Patiala, Punjab, India, 2014, pp. 649–651.
15 B. Ravel and M. Newville, *J. Synchrotron Radiat.*, 2005, **12**, 537–541.